ORNL/TM-2024/3373

Development of a self-lubricating high-efficiency hybrid seal composed of carbon nanotube-coated metal meshes for CSP turbomachinery

(SETO CSP #36333 Final Report)

Jun Qu
Chanaka Kumara
Lianshan Lin
Jim Keiser
Nguyen LaTray
Aida Rezaei
Tianlei Li
Alexander Urschel
Branden Pacer
Hunter Kramer
Fei Ren
Long Zhu

July 2024

OAK RIDGE National Laboratory

ORNL IS MANAGED BY UT-BATTELLE LLC FOR THE US DEPARTMENT OF ENERGY

ORNL/TM-2024/3373

Materials Science and Technology Division

DEVELOPMENT OF A SELF-LUBRICATING HIGH-EFFICIENCY HYBRID SEAL COMPOSED OF CARBON NANOTUBE-COATED METAL MESHES FOR CSP TURBOMACHINERY (SETO CPS #36333 FINAL REPORT)

Jun Qu, Chanaka Kumara, Lianshan Lin, and Jim Keiser
Oak Ridge National Laboratory

Nguyen LaTray, Aida Rezaei, Tianlei Li, Alexander Urschel, Branden Pacer, and Hunter Kramer
Danfoss

Fei Ren and Long Zhu
Temple University

April 2024

Prepared by
OAK RIDGE NATIONAL LABORATORY
Oak Ridge, TN 37831
managed by
UT-BATTELLE LLC
for the
US DEPARTMENT OF ENERGY
under contract DE-AC05-00OR22725

CONTENTS

ABSTRACT

In turbomachinery, internal leakage flow accounts for up to 3% of the total thermodynamic cycle energy loss. A tradeoff must be made between the sealing efficiency (smaller clearance) and the friction and wear issues for interfering with the shaft (larger clearance). This ORNL-Danfoss joint effort developed a novel hybrid seal composed of carbon nanotube (CNT)-coated metal meshes. The CNT growth process was based on a self-catalyzing chemical vapor deposition and these multiwall CNTs were well aligned with high crystallinity. This hybrid material structure takes advantage of the CNT's low-friction nature and uses the metal mesh as an extendable backbone. Full-scale experimental seals were designed and fabricated using different assembly and mounting approaches. Both bench-scale static and full-scale compressor seal tests were conducted, and the seal design was optimized based on the sealing performance, materials characterization, and contact mechanics simulation. The CNT-coated metal mesh seal demonstrated superior gas sealing efficiency to the baseline labyrinth seal and significantly improved shaft surface protection compared with the state-of-the-art superalloy brush seal on the static rig and full-scale compressor dynamometer tests. The CNT-metal mesh seal is low-cost and scalable and can potentially benefit wide applications, including concentrating solar power (CSP) and other power generation, marine, automotive, and heating, ventilation, and air conditioning (HVAC).

1. INTRODUCTION

1.1. Background

Internal leakage flow in turbomachines causes significant energy loss. For example, in current state-of-the-art turbomachinery, internal leakage flow accounts for up to 3% of the total thermodynamic cycle loss. During the past several decades, sealing technologies have undergone constant development and improvement. The state-of-the-art brush seal is an alternative to the conventional finned labyrinth seal and has demonstrated improved sealing capability and stability in turbomachinery. [1,2] A brush seal typically is made up of a stationary brush ring, which consists of densely packed bristles, bound by front and back plates. Typical operating conditions of brush seals are shown in Table 1. [3] To withstand the high temperature gas of a concentrated solar power (CSP) turbine, superalloy brush seal bristles have been introduced by the industry, such as H25 (Cr-Co-Ni) and Inconel718 (Ni-Cr-Fe). Other brush wires including aramide, Kevlar, and carbon fibers are also commercially available.

Table 1. Typical operation limits of the state-of-the-art brush seals [3]

Differential pressure	2.1 MPa
Surface speed	400 m/s
Operating temperature	600 °C
Size	3.1 m

For the commercial labyrinth and brush seals, a tradeoff must be made between the sealing efficiency (smaller clearance preferred) and the friction and wear issues for the seal interfering with the shaft spinning inside (larger clearance preferred). Current brush seals are designed with interference between the brush and shaft. Because the brush is in contact with the shaft, the risk of frictional drag–induced energy loss and wear is inevitable. Another drawback of the current brush seals is their high costs owing

to their complex manufacturing process. Compared with replacing a seal, the cost of refinishing or replacing a shaft is much higher. Therefore, a new, high-efficiency seal cannot sacrifice the shaft's durability.

1.2. Seal requirements and design parameters

Turbomachinery for supercritical CO_2 (sCO_2) power cycles falls into two major categories, turbines (expanders) and compressors. Within each major category, there are various configurations. In order to develop seals applicable to sCO_2 system, Danfoss consulted Ecogen Power System (EPS) for seal design criteria. Operating conditions for seals on the external shaft, turbine, low-temperature compressor (LTC), and high-temperature compressor (HTC) are summarized based on EPS' current sCO_2 system design. [4]

The process conditions at the turbine depend on the operating conditions of the specific application, but in general, the inlet pressure ranges 20-30 MPa, and the inlet temperature is 400-700 °C, and the exit pressure is 5-8 MPa. The exit temperature typically is 150-200 °C lower than the inlet temperature. The compressor operates over a similar pressure range (5-8 MPa at the inlet, 20-30 MPa at the exit). The inlet temperature for LTC ranges 20-50 °C, with the outlet temperature about 10-30 °C higher than the inlet. The inlet temperature for the HTC can vary from 65 to 150 °C, with the outlet 30-50 °C hotter.

From the operating conditions in the EPS system, the project team identified three categories of seals at different locations. The operating conditions for each category are shown in Table 2. The seal inlet pressure and temperature are listed, and the seal outlet pressure and temperature can be estimated with the assumption of isenthalpic expansion. [5-7] In category one, seals are used on the LT and HT compressor interstage shaft and impeller eye seals. The temperature and pressure difference across the seals in this category is relatively low which leads to flexibility in the sealing technologies and materials which may be used. [8] In the second category, the seals are used on the turbine shaft. The operating pressure is similar to category one, but the temperature is much higher. This will impose higher requirements on the seal materials. In the third category, the seal is used for a system with a single turbine or compressor. The seal in this case experiences high pressure and temperature in the operation.

This project focuses on developing cost-effective high-performance seals for category one to demonstrate the concept. An example of calculated seal operating conditions in a 4-stage compressor is given in Table 3, for an inlet condition of 7.5 MPa, 30 °C, and outlet conditions of 25 MPa and 55 °C.

Table 2. General requirements for seals in sCO_2 turbine and compressor systems

Seal requirements, 10-100 MW system	Max Upstream inlet P (MPa)	Max Upstream inlet T (°C)	Max Pressure ratio	Max seal ID (mm)	radial clearance (mm)	Max shaft normal vibration* (mm)	Max shaft excursion	Max surface speed (m/s)	Max kRPM
Interstage compressor shaft/eye seals (HT and LT), 2-4 compressors	30	200	2	900	0.1-0.25	0.025	<75% of clearance	250	75
Interstage turbine shaft seals, 2-4 turbines	30	800	2	400	0.1-0.25	0.025	<75% of clearance	80	75
Single stage seal, single turbine or compressor	30	800	4	650	0.1-0.25	0.025	<75% of clearance	350	150

**Based on API617 standard*

Table 3. Examples of end seal operation conditions in a 4-stage compressor

	Upstream P (MPa)	Downstream P (MPa)	PR	dP (MPa)	Upstream T (°C)	h (kJ/kg)	Density (kg/m^3)	Downstream T (°C), isenthalpic
1st stage	9.5	7.5	1.3	2.0	45.8	377.6	386.8	32.7
2nd stage	13.5	11.4	1.2	2.1	50.6	324.3	649.1	45.8
3rd stage	17.8	15.6	1.1	2.2	53.2	313.2	731.8	50.6
4th stage	22.3	20.0	1.1	2.3	55.0	307.9	783.3	53.2
Shaft Seal	16.3	7.5	2.2	8.8	55.0	323.5	687.2	31.6

1.3. Carbon nanotubes for a low-clearance and low-friction seal

Carbon nanotubes (CNTs) are made up of one or more graphene sheets concentrically rolled-up into cylindrical tubes. CNTs have been used as composites, [9] electrode materials, [10,11] solar cells, [12] and gas sensors [13] due to their unique mechanical and chemical properties. CNTs have a high surface area due to their tubular structure and high aspect ratio, which allows them to trap, store, and separate liquids and gases. [14-16] Additionally, due to their high graphene content, CNTs were reported with excellent tribological properties, making them useful for reducing friction and wear. [17-19]

Three techniques commonly used to grow CNTs are arc discharge, laser ablation, and chemical vapor deposition (CVD). Among these techniques, CVD is the most widely used with catalysts. [20] The catalyst nanoparticles for converting carbon materials to CNTs include Fe, Ni, and Co due to their high solubility and diffusion rate for carbon atoms at high temperatures. The catalyst particles are often added externally as a thin atomic layer onto the substrate using methods like e-beam, atomic layer deposition or sputtering. [21] For example, vertically aligned dense CNTs could be grown on steel, such as stainless steel, by deposition of the Fe layer. [22] The CNTs could also be grown on steel substrates without

externally deposited catalysts. In this case, the substrate element composition plays a leading role in generating nanoscale catalyst particles in situ. [23-25]

In this project, we developed a self-catalyzing CVD process [26] for growing CNTs on a stainless steel mesh. This hybrid material structure (CNT-coated metal mesh) was then used to construct a novel seal [27] by taking advantage of the CNT's low-friction nature and using the metal mesh as a literally unlimitedly extendable backbone for improved sealing efficiency, compliance, and durability.

2. CNT GROWTH AND CHARACTERIZATION

2.1. CNT growth

ORNL developed a chemical vapor deposition (CVD) process to produce an array of vertically aligned CNTs on a ferrous alloy surface. [26] Our CVD process has two key features: (i) Unlike conventional methods that require spraying catalytical nanoparticles on the surface to grow CNTs, this method does not need any add-on catalyst and is referred to as 'catalyst-free' or 'self-catalytical' here, and (ii) Unlike the randomly oriented CNTs grown by conventional methods, ORNL CNTs are vertically aligned.

The small CVD setup is shown in Figure 1a and the process is illustrated in Figure 1b involving four steps to grow CNTs: (1) oxidation in air under sub-atmospheric pressure, (2) reduction in a gas environment, e.g., Ar/H_2, (3) CNT growth in a carbon source, e.g., ethanol (EtOH), and (4) cooling down under Ar/H_2 flow. In this process, the alloy surface is first oxidized and then reduced, essentially creating catalytical nano-scale features on the surface to initiate the growth of CNTs.

The key CVD process parameters include gas environment, temperature, pressure, which were optimized to improve the CNT length and surface coverage of the substrate. Table 4 outlines the parameters used for the CNT synthesis. All the CVD parameters play a collective role in CNT growth, but it was found that the CVD temperature and air oxidation were the two most critical parameters. Experiments performed at 750 and 700 ^oC generated 10-15 μm long CNTs with excellent coverage on the metal surface. Furnace temperatures at 650 and 600 ^oC also produced good surface coverage of CNTs, but the CNT length was less than 5 μm.

(a)

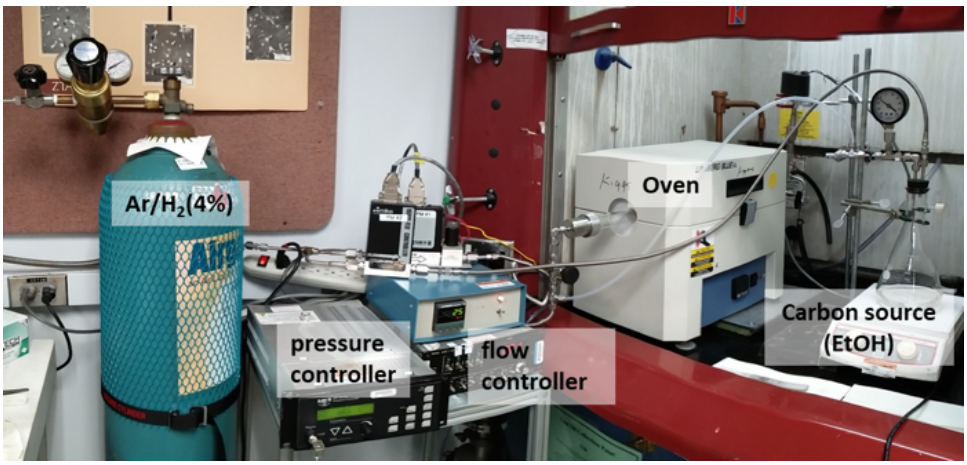

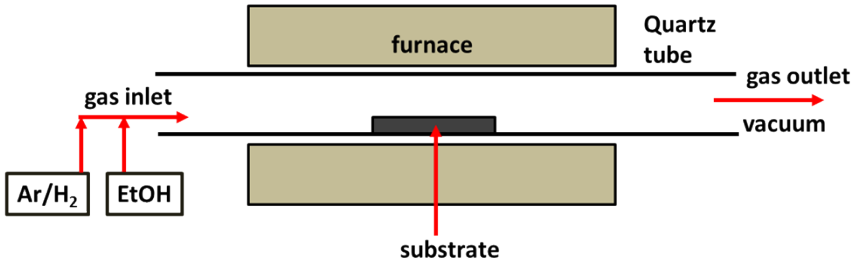

Figure 1. ORNL 'self-catalytical' CVD process for growing vertically-aligned CNTs.

Table 4. CNT growth under different CVD process conditions

Temp. (°C)	Air flow pressure (torr)	Ar + 4% H_2 introducing time (min)	Reduction pressure (Torr)	Ar + 4% H_2 flow rate (ccm)	EtOH introducing pressure (torr)	EtOH exposure time (min)	Surface coverage by CNTs
800	300	30	600	500	<10	15	None
750	300	30	600	300	<10	15	OK
700	300	30	600	300	<10	30	Good
650	300	30	600	400	<10	15	OK
600	300	30	600	500	<10	15	Poor
700	**120**	**60**	**600**	**500**	**<10**	**15**	**Excellent**

CNTs were first grown on Type 316 stainless steel (SS) samples with both flat and curved surfaces. Figure 2a shows a Type 316 SS disk before and after the CVD process. The entire surface appears to be black after the process indicating a good coating coverage. SEM examination showed a vertically aligned CNT array on the SS surface. The lengths of the CNTs vary from 10 to 40 µm depending on the synthesis conditions. The diameters of the CNTs are 40-50 nm. In addition to flat surfaces, a 316 SS wire mesh was used for testing CNTs' growth on curve surfaces. Initial results are shown in Figure 2b. The wires became black after the CVD process indicating the formation of CNTs. SEM images show evidence of good surface coverage of CNT arrays. We have also demonstrated the feasibility of growing CNTs on D2, A2, and H13 tool steels using the 'self-catalytical' CVD process.

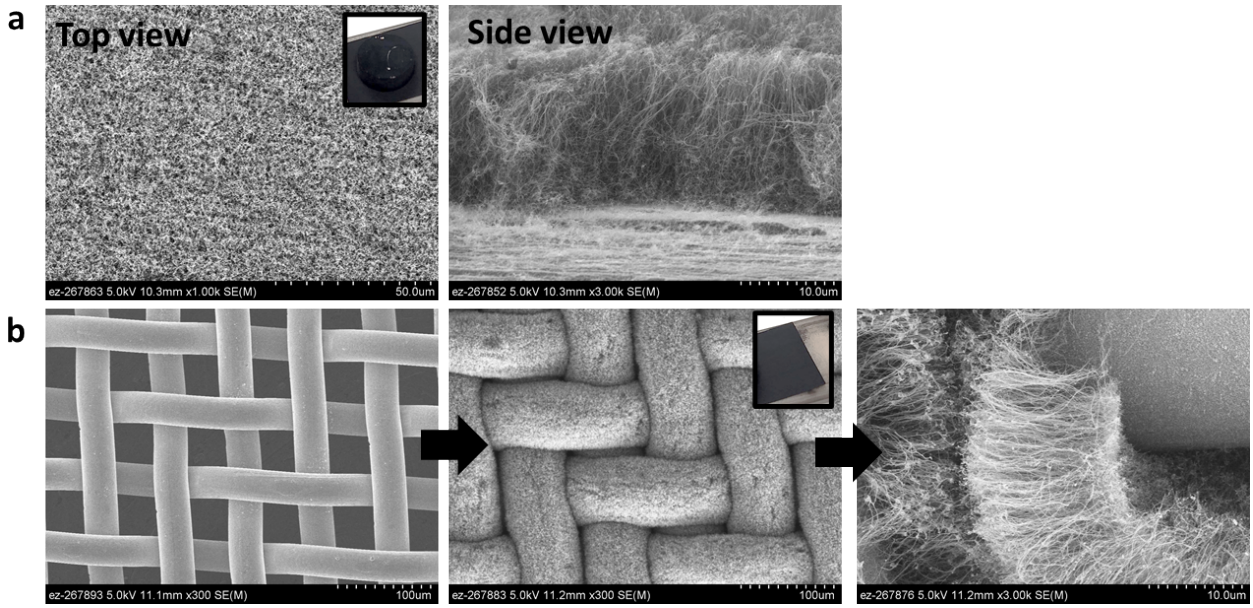

Figure 2. CNTs grown on Type 316 stainless steel disk (a) and mesh (b). The SEM image to the right shows the area where CNTs were intentionally scraped from the surface for imaging.

2.2. Low friction characteristics of the CNTs

Disk-on-flat reciprocating sliding (see Fig. 3a) tests were conducted in dry conditions. A Type 316 SS disk (9.98 mm diameter) with or without CNT coating was used to rub against a M2 tool steel flat (25.4 mm diameter). All tests were carried out at room temperature under a constant 100 N load at 0.5 Hz oscillation with a 10 mm stroke for 100 m sliding (~166 mins). SS disks in three forms were tested: as polished, CNT-coated, and heat treated by going through the CVD process but without introducing the carbon source. Figure 3b compares the friction results. Both control tests on the SS disks without CNTs were forced to stop after a short sliding distance (< 25 m) due to the friction coefficient being too high (>0.8) and squeaking noise. In contrast, the CNT-coated disk maintained a friction coefficient of around 0.2 which is a 75% reduction compared to the control.

The deposition of a transfer layer was clearly visible on both the SS and M2 steel surfaces. Raman analysis suggested that such a transfer film is carbon-based and contains a significant amount of graphene oxides, which may be responsible for the low friction behavior.

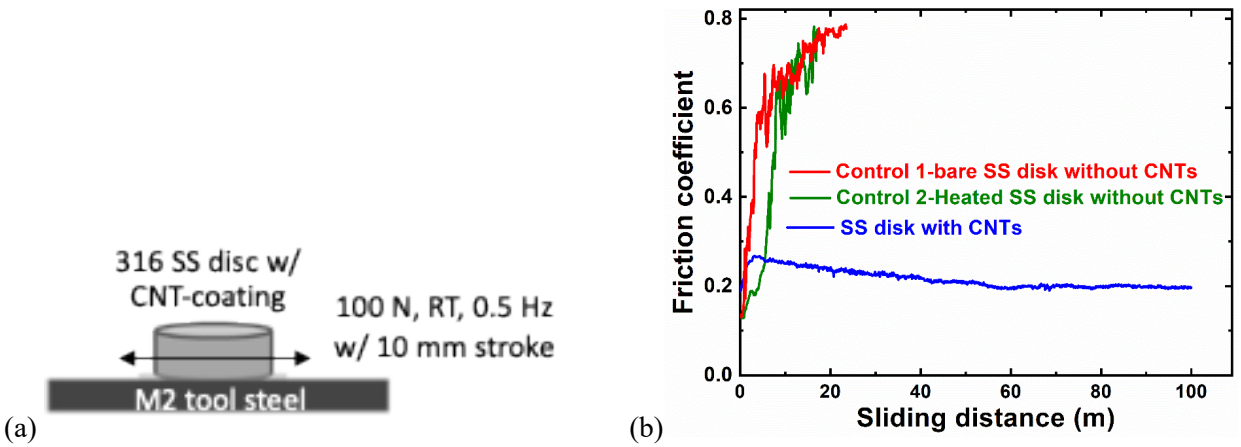

Figure 3. CNT array prevented scuffing and produced significantly lower friction than the surface without CNTs in dry sliding. (a) Schematic of disk-on-flat sliding test and (b) Comparison of friction traces of SS disks without and with a CNT coating.

2.3. Constructing a larger CVD system to accommodate actual seal base structures

A larger CVD system was designed and assembled to accommodate the CSP compressors' actual seal base structures, as shown in Figure 4**.** This new CVD tube has an inner diameter of 88.9 mm and a heat zone of 400 mm (length). Necessary safety components were installed to ensure safe operation. CNTs were successfully grown on the inner wall of a full-size (66 mm inner diameter) seal base as shown in Figure 5. After realizing the technical challenges of the limited CNT length and weak bonding strength to the substrate, we dropped the original approach of using CNTs as brush seal bristles. Instead, we invented the new CNT-coated metal mesh hybrid seal, as described in Section 3.

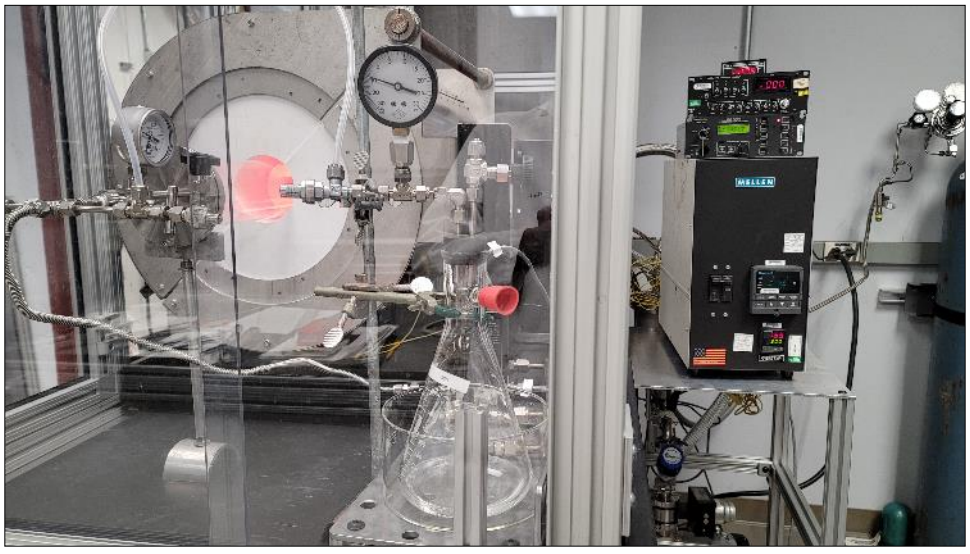

Figure 4. ORNL's new designated larger-size CVD system for growing CNTs to accommodate actual seal base structures for CSP compressors.

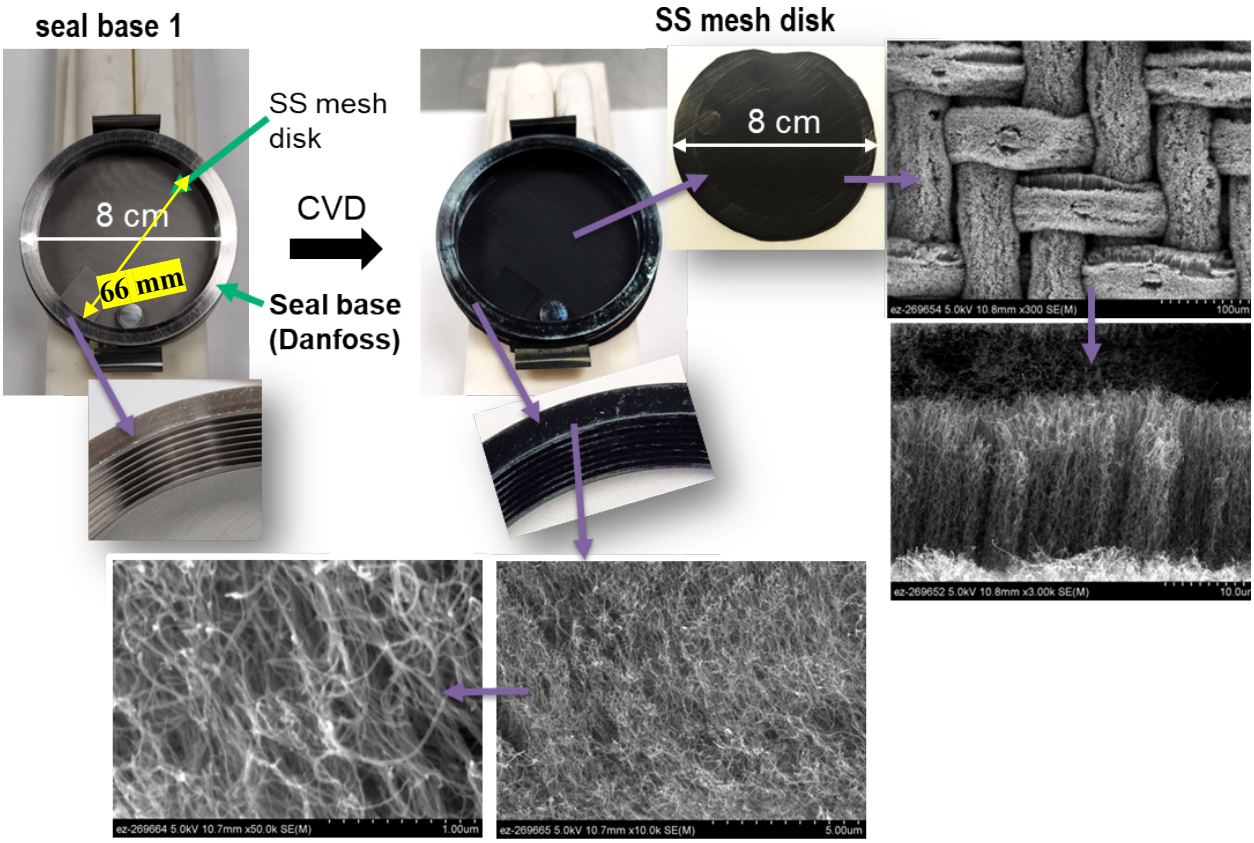

Figure 5. Feasibility demonstration of growing CNTs on an actual seal base (from Danfoss) and a set (6) of SS mesh disks using the larger CVD system. Expansions show the grooves on the inner wall of the seal base as well as the mesh wires before and after the CVD process.

2.4 CNTs' crystallinity

Figure 6 shows the *Raman* map of a CNT array (including around 900 CNTs) at multiple locations from the top to the bottom, with data collected at 1 μm steps. Figure 6a shows an array of CNTs on a Type 316 stainless steel mesh. Figure 6b shows the *Raman* map reflecting the intensity distribution of the graphene band along the length. Figure 6c shows three *Raman* spectra collected near the bottom (closer to the substrate), middle, and top of the CNT array. Figure 6d shows the intensities of the G and D bands along the CNT height. The ratio of the G to D band (I_G/I_D) is more than 2, indicating a relatively high degree of crystallinity.

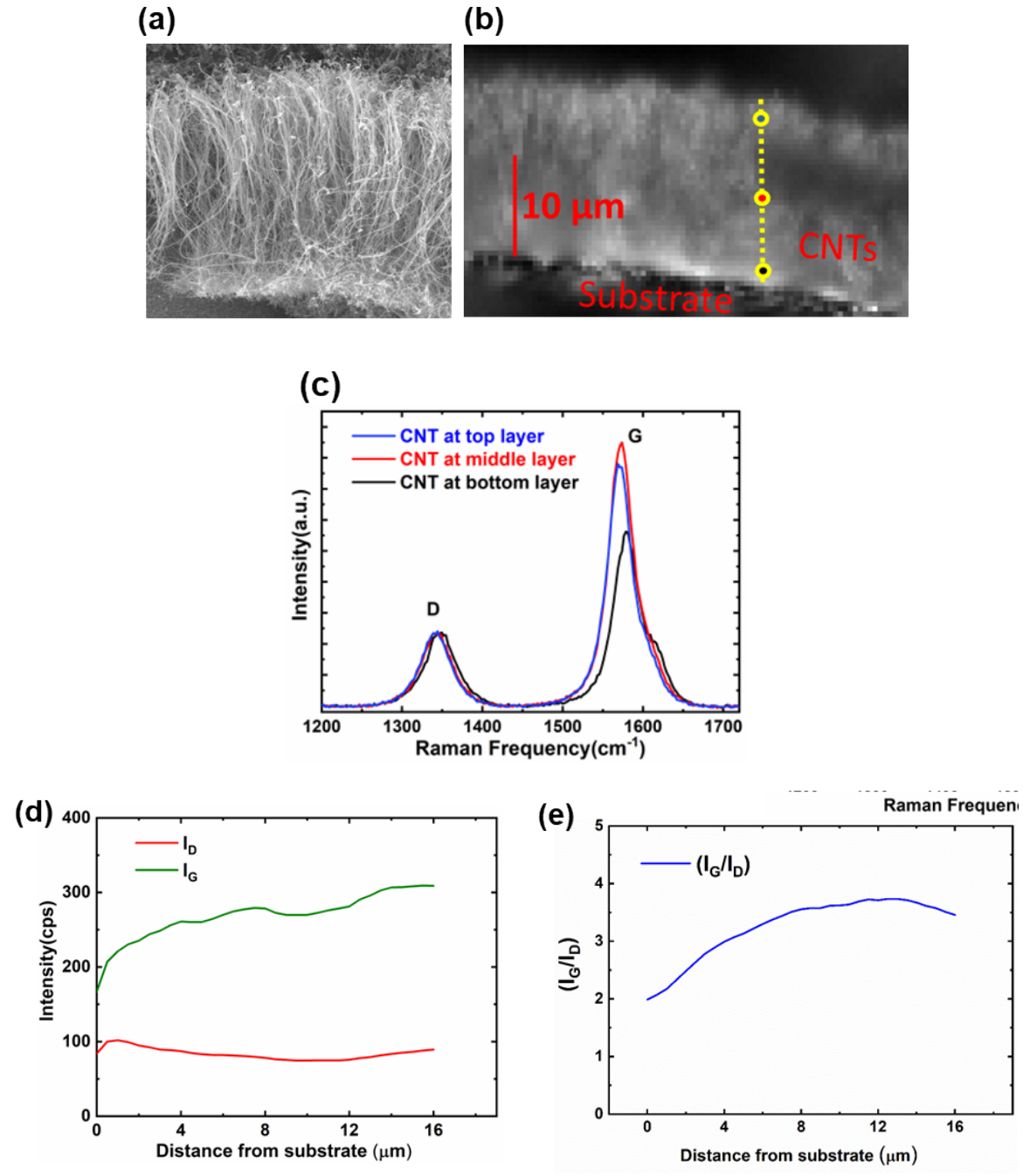

Figure 6. *Raman* spectroscopy analysis of an array of CNTs grown on a stainless steel mesh. (a) SEM image of the CNTs, (b) *Raman* map showing the intensity distribution of graphene band, (c) *Raman* spectra of the CNT array at near the bottom, middle, and top, (d) Intensities of the G and D bands along the length of the CNT array, (e) I_G/I_D ratio of the CNT array along the length. *Raman* spectra were collected at each 1 µm.

2.5. CNTs in sCO_2 corrosion tests

According to the API 617 standard for seal requirement of supercritical CO_2 (sCO_2) turbine and compressor systems, maximum upstream inlet pressure could reach up to 30 MPa. The maximum upstream inlet temperature could reach 200 and 800 °C for the interstage compressor and turbine shafts, respectively. (See Table 2)

To understand the compatibility of the CNT-coated SS mesh with the sCO_2 environment, Type 316 SS meshes without and with CNTs were exposed to research-grade sCO_2 (<5 ppm O_2, <5 ppm H_2O) at 200, 400, and 750 °C and under 20-30 MPa pressure for up to 500 hours in a vertically oriented autoclave machine with ceramic specimen rack. Figure 7 shows the corrosion test setup and control system. The autoclave was heated inside with a three-zone furnace, and the fluid flow rate was maintained at ~2 mL/min. The specimens were heated in sCO_2 to the target temperature under the heating rate of ~2°C/min, held at temperature ±2°C for 500 hours, and then cooled in sCO_2 to the room temperature. The maximum operation temperature of our system was limited to 750 °C. Three tests were conducted: Test 1 was terminated after 141 hours because of difficulties in maintaining the 20 MPa pressure at 200 °C. No pressure problem was encountered at 400 °C (Test 2) or above 700 °C (Test 3) and thus those two tests completed the full course of 500 hours. In Test 3, because of the temperature gradient, the samples hung on the rack near the top, at the middle, and near the bottom experienced 718, 740, and 750, respectively. Note: the top of the autoclave was exposed to the ambient environment and thus was cooler than the bottom which was fully surrounded by the furnace.

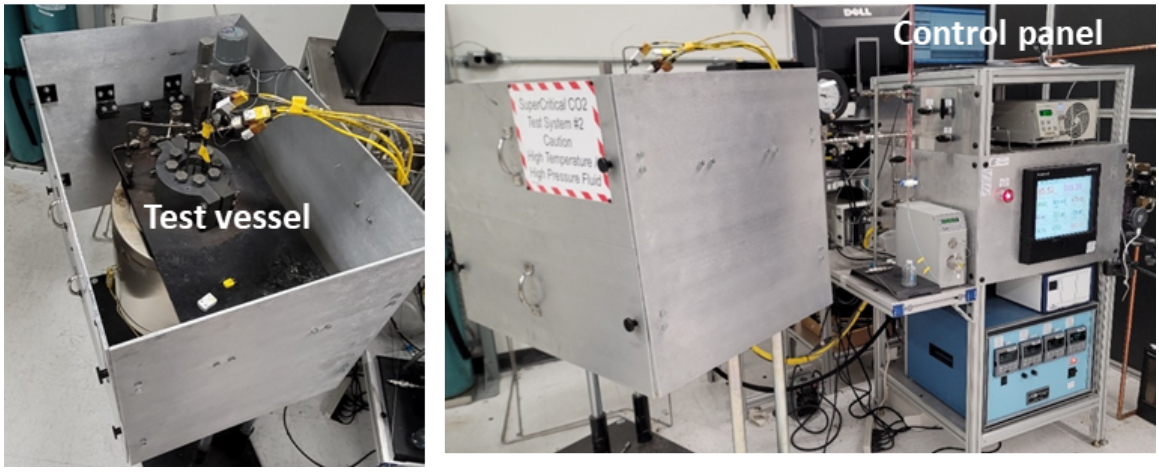

Figure 7. sCO_2 corrosion test vessel and control system.

Figures 8 and 9 show the morphologies of the bare and CNT-coated stainless steel meshes before and after the corrosion tests, respectively. Both bare and CNT-coated meshes showed little morphological change after the tests at 200 and 400 °C. In contrast, the bare stainless steel mesh surface after the test at 750 °C in sCO_2 showed heterogeneous bristles of 5-15 μm in length (see Figure 8 right-bottom). EDS elemental maps in Figure 10 showed high oxygen and iron contents of these bristles, suggesting iron oxides as a result of chemical reactions with sCO_2. The significant corrosion of the stainless steel substrate is believed to cause the loss of CNTs from the CNT-coated mesh in the 750 °C sCO_2 test. The EDS elemental maps confirm that the needle-like surface structures are predominantly comprised of Fe and O, as shown in Figure 9.

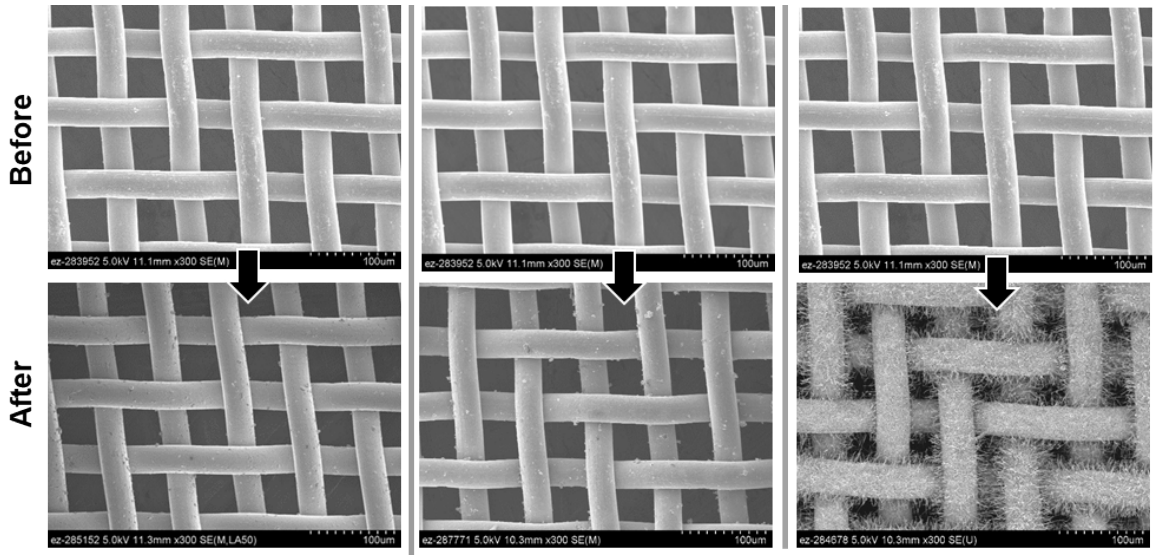

Figure 8. Bare Type 316 stainless steel meshes (325x325) after sCO_2 corrosion tests at 200 °C (left), 400 °C (center), and 750 °C (right).

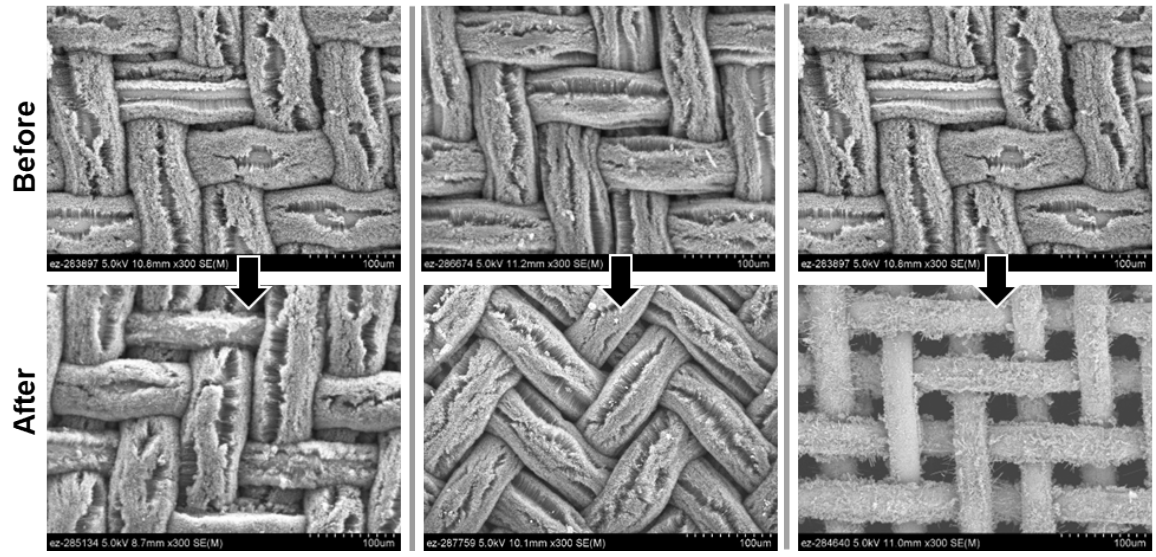

Figure 9. CNT-coated Type 316 stainless steel meshes (325x325) after sCO_2 corrosion tests at 200 °C (left), 400 °C (center), and 750 °C (right).

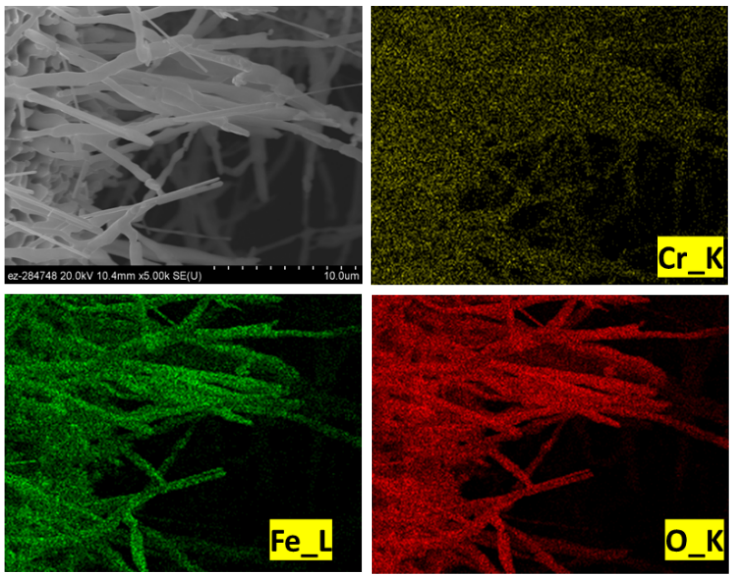

Figure 10. EDS elemental maps of the bare Type 316 SS mesh after the corrosion test at 750 °C

3. SEAL DESIGN AND FABRICATION

3.1. Design concept of a CNT-coated metal mesh seal

The design concept for the CNT-coated metal mesh seal is illustrated in Figure 11. This hybrid seal has the following advantages over state-of-the-art seals and can be applied to turbomachines, thereby benefiting wide applications, including CSP.

- **Improved sealing efficiency.** The self-lubricating CNTs allow a nominal zero clearance to the shaft with little risk of wear damage on the seal or the shaft. As a result, it significantly reduces the internal leakage flow and frictional loss to improve the turbomachinery's efficiency.
- **Low friction and low shaft wear**. The self-lubricating characteristic of the CNTs reduces friction and protects the shaft from damage.
- **Reduced manufacturing cost.** The fabrication of the CNT-based seals is scalable in seal size and production volume and the manufacturing cost is estimated to be significantly lower than the state-of-the-art brush seals.

Two routes were proposed and trialed for fabricating and assembling the CNT-coated metal mesh seal and their advantages and disadvantages are compared in Table 5.

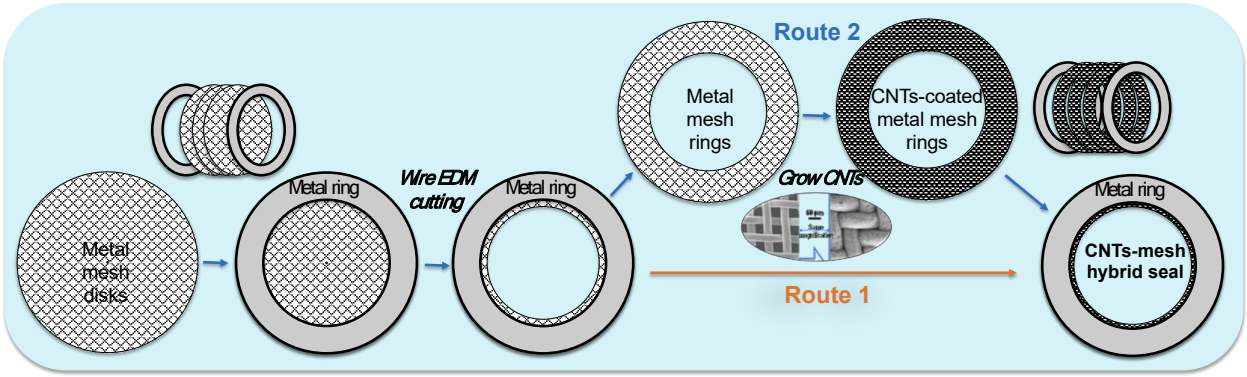

Figure 11. Design concept of the CNT-coated metal mesh seal.

Table 5. Comparison of the advantages and disadvantages of Routes 1 and 2.

	Key features	Advantages	Disadvantages
Route 1	Coating CNTs on the full assembly	• Simpler process • Better concentricity among mesh layers	• Difficulties in CNT growth • Seal OD size limited by the CVD furnace ID
Route 2	Coating CNTs on the mesh layers	• Longer CNTs & better surface coverage • Seal OD size up to 2-5X of the CVD furnace ID	• Disassembly & reassembly for CNT growth

3.2. Fabrication of experimental CNT-coated metal mesh seals

The first trial seal fabricated using the Route 1 process is shown in Figure 12. A stack of 12 layers of Type 316 stainless steel meshes was used. As shown in Figure 12, the CNTs on the mesh are found to be short and have poor surface coverage. Two problems were identified: (1) full seal assembly restricted gas flow between the layers of mesh in the CVD process and (2) machining debris adhering onto the SS meshes and suppressing CNT growth.

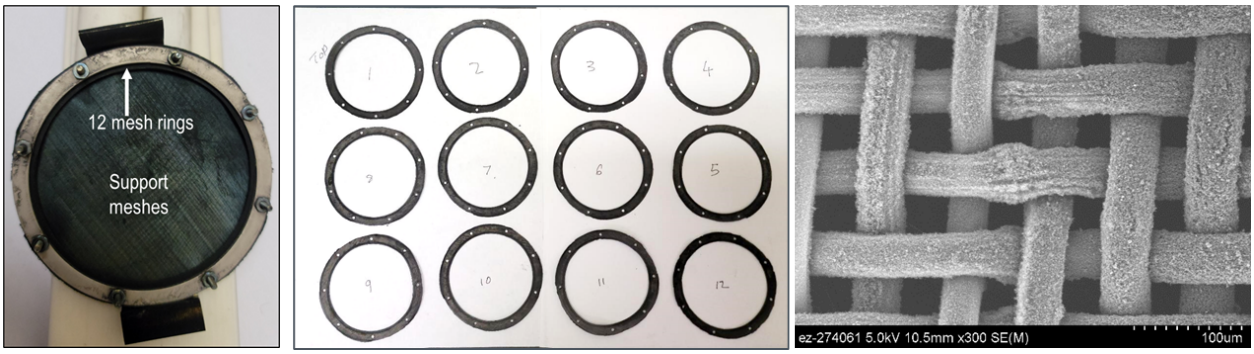

Figure 12. A trial CNT-metal mesh seal using the Route 1 process (coating CNTs on the full assembly, as illustrated in Figure 12). CNTs on the stainless steel mesh are short and have poor surface coverage.

The seal fabrication using Route 2 (see Figure 11) is shown in Figures 13 and 14. The machining debris was found to adhere onto the metal meshes and suppress the CNT growth. Several methods were tried to clean the SS mesh rings after cutting. Acid treatment was discovered to be effective in cleaning the mesh by oxidizing the metal debris and dissolving the oxidation products in aqueous solutions. In this trial, the mesh rings were folded into half circles before being inserted into the CVD tubing chamber. This not only allows the process gas to effectively flow through the meshes but also makes it possible to treat mesh rings with OD larger than the CVD tubing ID. If smartly rolled, the mesh ring OD could be as large as 2-5X of the CVD tubing ID (3X for a single roll and 5X for a double roll). Figures 13b and 13c show a stack of twelve 325x325 mesh rings before and after the CVD process. All mesh rings appear to have good CNT coverage and the openings are literally sealed by the CNTs, as shown in Figure 13d.

An assembly tool was designed and made to control the concentricity for assembling the CNT-coated mesh rings, as illustrated in Figures 14a and 14b. Figure 14c displays the full assembly of the trial CNT-metal mesh seal with 12 layers of CNT-coated stainless steel meshes. The zoom-in optical image in Figure 14d clearly shows the good sealing of mesh openings by the CNTs.

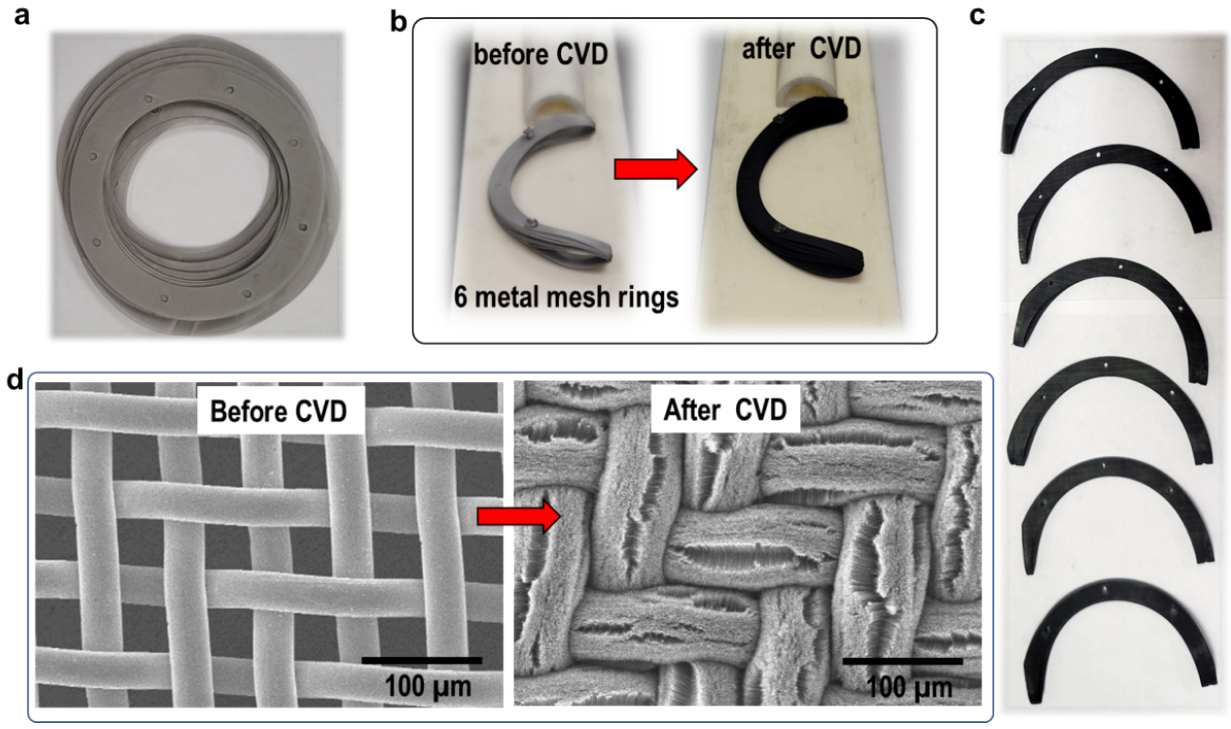

Figure 13. First trial of Route 2 (coating CNTs on the metal meshes, as illustrated in Figure 11). (a) Stainless steel mesh rings; (b, c) Metal mesh rings before and after the CVD process; (d) SEM images of the mesh before and after CNT growth.

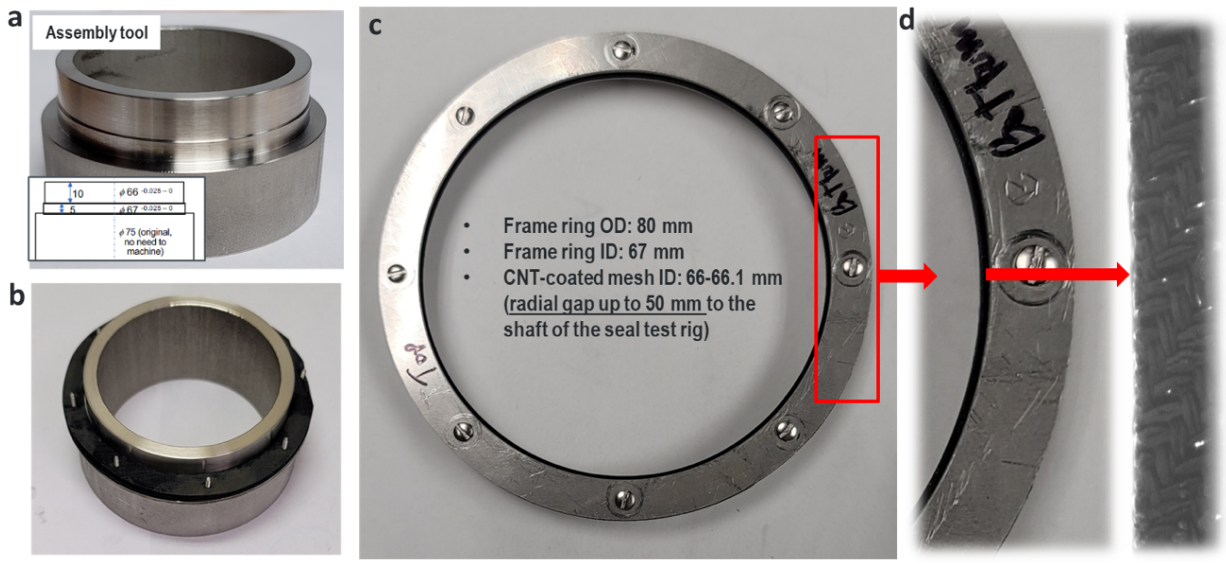

Figure 14. Full assembly of a trial CNT-coated mesh seal using Route 2. (a,b) Assembly tool to control the concentricity among the CNT-coated mesh rings; (c) Full assembly (ID: 66 mm); (d) Zoom-in optical image showing CNTs sealing the mesh openings.

The second version of the CNT-coated metal mesh seal had better compatibility with the seal test rig and compressor, e.g., having a flat surface to allow easier installation and the same OD as the commercial brush seals. Figure 15 shows the experimental CNT-coated metal mesh seal fabricated using the improved design above. It contains 24 CNT-coated stainless steel mesh layers. All mesh layers appear to have good CNT coverage and the mesh openings are literally sealed by the CNTs.

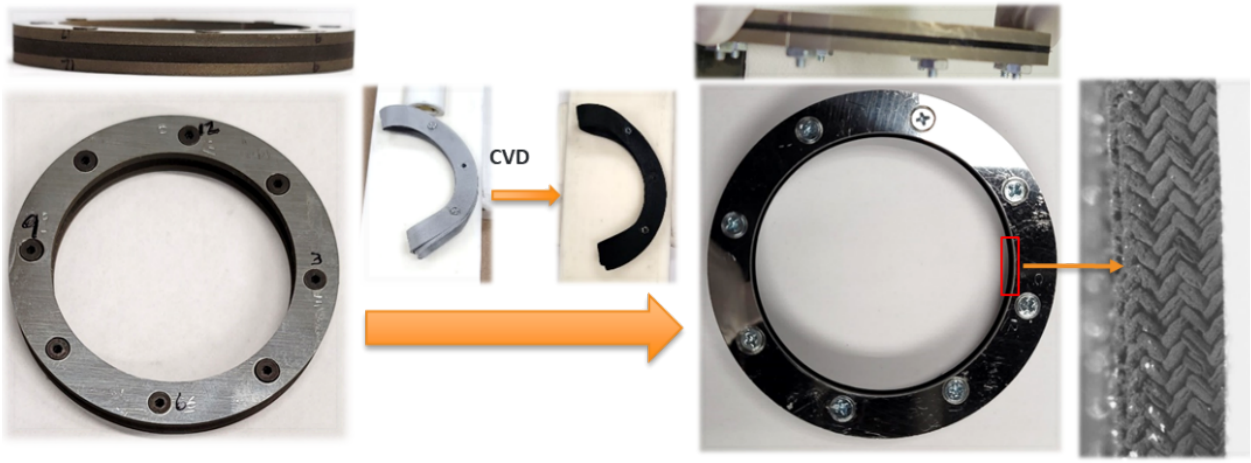

Figure 15. An experimental CNT-metal mesh seal of the improved design (version 2), which has a nominal OD of 88.9 mm (same as commercial brush seals), a nominal ID of 66.0 mm, 24 layers of CNT-coated stainless meshes, and a flat surface to better fit with the seal test rig and compressor.

4. SEAL TESTING RESULTS

4.1. Static seal rig testing

A static seal test rig with a 66 mm diameter shaft was set up at Danfoss, as shown in Figure 16. The test seal confines air in an enclosure that maintains both upstream and downstream pressures. The downstream leaks to the ambient. A flowmeter was used to measure the air mass flow passing the seal at various pressure differentials.

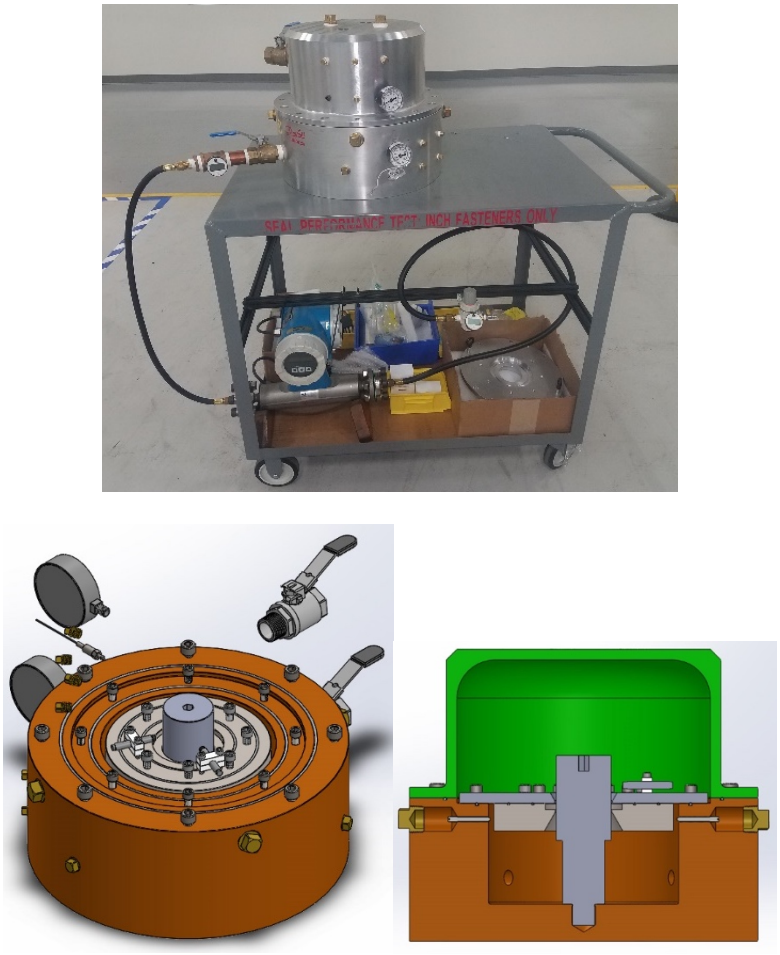

Figure 16. A static seal testing rig. The test labyrinth seal confines air in an enclosure that maintained pressure at both up and down streams. The downstream leaks to the ambient. A flow meter is used to measure the air mass flow passing the seal at various pressure differentials.

Danfoss conducted static seal rig tests of the two experimental CNT-metal mesh seals shown in Figures 16 and 19. Two baseline labyrinth seals and three state-of-the-art brush seals were acquired for comparison against the new CNT-coated metal mesh seal. All seals were designed for the 66 mm diameter shaft. The two labyrinth seals had radial clearances of 0.08 and 0.14 mm, respectively. The three

brush seals use metallic, polymeric, and carbon fiber bristles, respectively. The brush seals were acquired from commercial vendors for either the aerospace or nuclear power industry. The Haynes alloy bristles are 1 mm thick and have nominally no clearance or overlap with the shaft, the carbon fibers are several mm thick and have a significant overlap, and the Kevlar fibers are several mm thick and have a small overlap.

The static seal test results are summarized in Figure 17. Key observations are:

- The version-2 CNT-coated metal mesh seal had >75% less leakage flow than the superalloy brush seal.
- The version-2 CNT-coated metal mesh seal showed increasingly better sealing efficiency than the Kevlar brush seal along with the pressure ratio (PR), e.g., 40% improvement at the PR of 5.
- The version-2 CNT-coated metal mesh seal with the assembly screw holes sealed by superglue showed significantly higher sealing efficiency than the version-1, but these two seals performed similarly otherwise. This leads to further improvement in the seal design using screw counterholes for assembly.
- The carbon fiber brush seal had slightly better sealing than the CNT-metal mesh seal because of its much larger radial overlap, but it experienced severe bristle damage in the compressor dyno test.

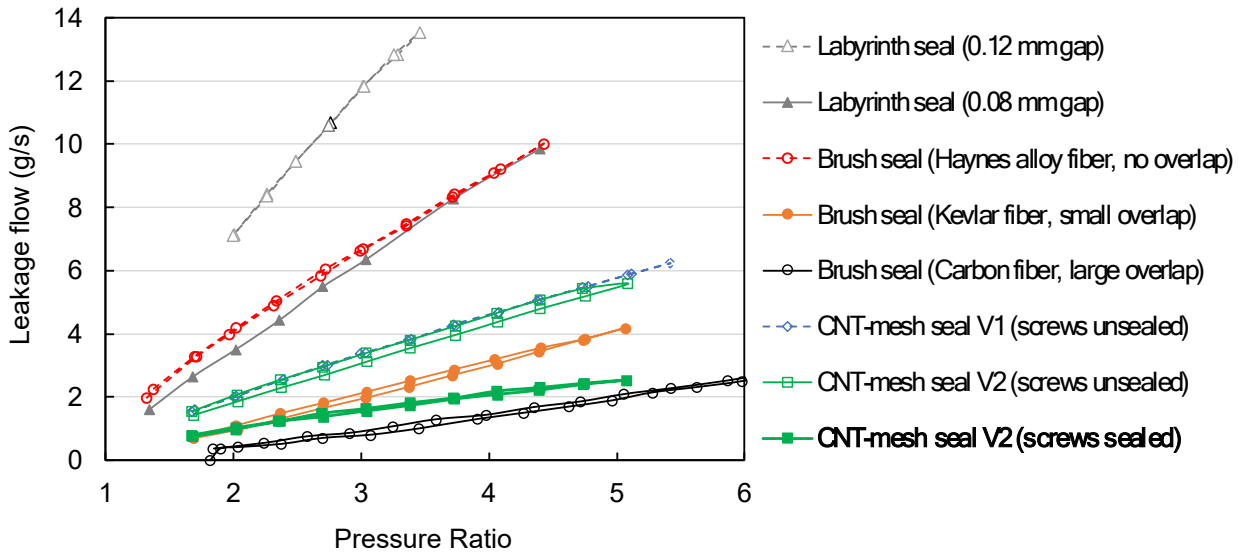

Figure 17. Static seal rig testing results of the CNT-coated metal mesh seals in comparison with those of commercial labyrinth and state-of-the-art brush seals. The CNT-coated metal mesh seal had >75% less leakage flow than the superalloy brush seal and increasingly better sealing efficiency than the Kevlar brush seal along with the pressure ratio (PR), e.g., 40% improvement at PR of 5.

4.2. Compressor dynamometer seal testing

The version-2 seal containing 20 layers of CNT-coated 325x325 stainless steel mesh went through a durability test on a full-scale compressor dynamometer. The seal was mounted using screws (fixed mounting). The test duration was more than 34 hrs under a pressure of up to 1690 KPa and a speed 15,500-32,000 rpm in a gas environment of refrigerant R134A at temperatures up to 82 ^{o}C (see Table 6).

Table 6. Compressor dynamometer durability seal test conditions

Extreme conditions	Speed [RPM]	31,992.9
	Pressure [kPa]	1690.3
	Temperature [^{o}C]	82
Multiple speeds between 15500 and 32000 RPM	Total Run Time	34 hours 28 minutes
	Gas	Refrigerant R134A

The CNT-coated metal mesh seal after the compressor durability test is shown in Figure 18. Plastic deformation and wear were observed on the seal inner diameter (ID) as a result of inevitable contact against the rotating shaft due to runout and vibration, though the damage is still less than that experienced by the commercial carbon fiber brush seal after the compressor durability test (see the fiber fractures in Figure 19). No surface damage was observed on the shaft (see Figure 18). The shaft clearly shows a layer of carbon transfer film on the region rubbing against the seal, which is expected to produce low friction and protect the shaft surface. In contrast, the commercial superalloy brush seal caused lots of scratches on the shaft surface during the compressor test.

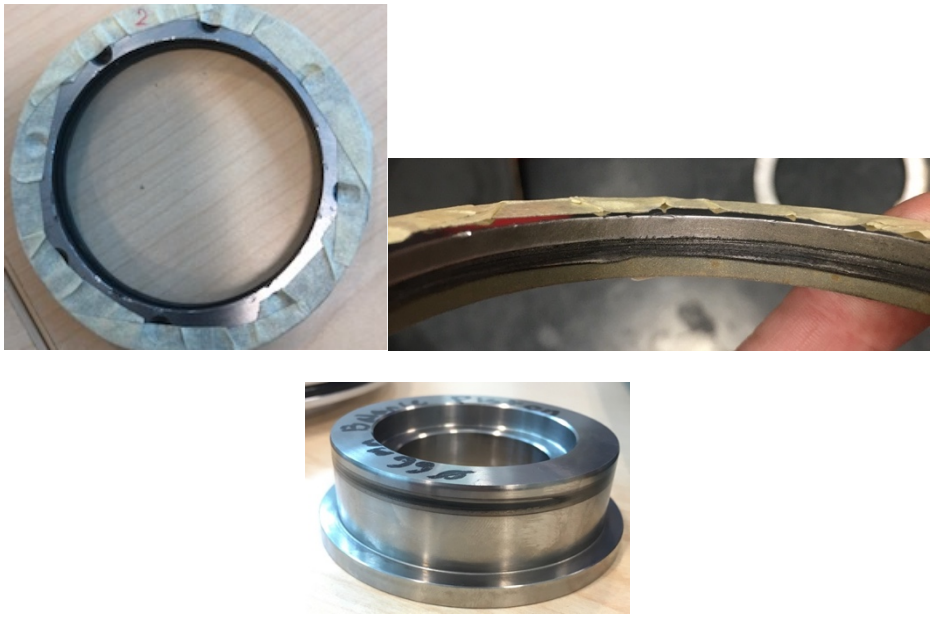

Figure 18. The CNT-coated metal mesh seal (top, ID: 66 mm) and the mating shaft (bottom) after a 43.5-hr compressor durability test using fixed seal mounting. Plastic deformation and wear observed on the seal ID. A layer of carbon transfer film seen on the shaft (no surface damage).

Figure 19. Commercial carbon fiber brush seal showing significant fiber fractures after a compressor durability test.

The ID damage of the CNT-coated metal mesh seal (see Figure 18) was in part attributed to the fixed mounting approach that cannot tolerate the shaft's runout, vibration, or radial movement when switching between the roller bearings and magnetic bearings at startup and shutdown. For a fixed mounted labyrinth seal, a >100 μm radial gap is required as illustrated in Figure 20 (left). An alternate floating mounting was proposed for the CNT-coated metal mesh seal, as shown in Figure 20 (right). In such a scenario, the seal is supposed to move along with the shaft's radial movement to reduce the contact pressure on the seal ID and consequently the plastic deformation and wear.

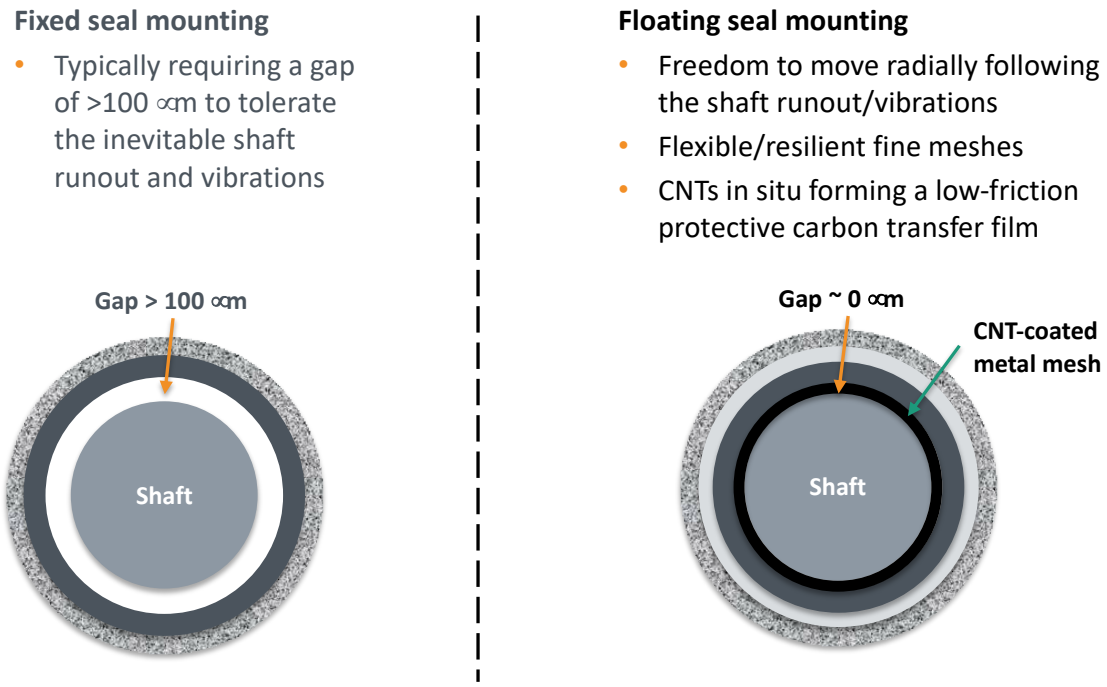

Figure 20. Floating seal mounting for reducing the ID damage of the CNT-coated metal mesh seal.

Multiple trials of the seal and volute designs were experimented with for the floating mounting approach before passing the 5-min open-air test on the compressor. The latest version of the CNT-coated metal mesh seal (20 layers of mesh) before the compressor test is shown in Figure 21.

The seal passed the open-air test and then went through a 160-hr compressor durability test with a shaft speed of 31,000 rpm for 66 hrs and then 27,000 rpm for 94 hrs under a pressure ratio of 4.6 in a R-134A environment at a saturated suction temperature of 5°C. The tested seal and shaft are shown in Figure 22. No surface damage was observed but a carbon transfer film was detected on the shaft surface. Also, no obvious plastic deformation was seen on the seal ID, significantly less damage compared with the seal tested using fixed mounting (see Figure 18). The seal ID was determined to be enlarged by 0.37 mm based on the measurements at new conditions and then after the compressor tests.

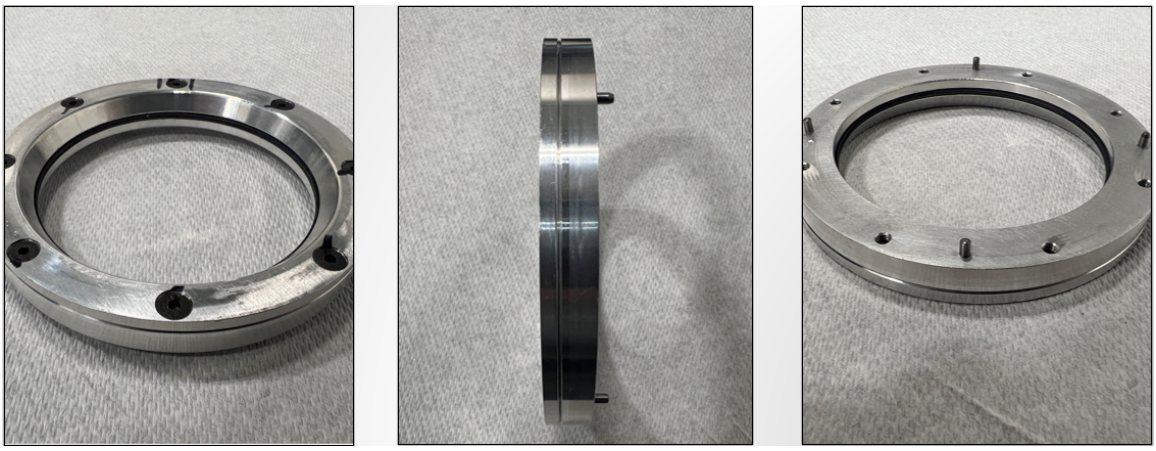

Figure 21. An experimental CNT-metal mesh seal (ID: 66 mm) designed and fabricated for floating mounting.

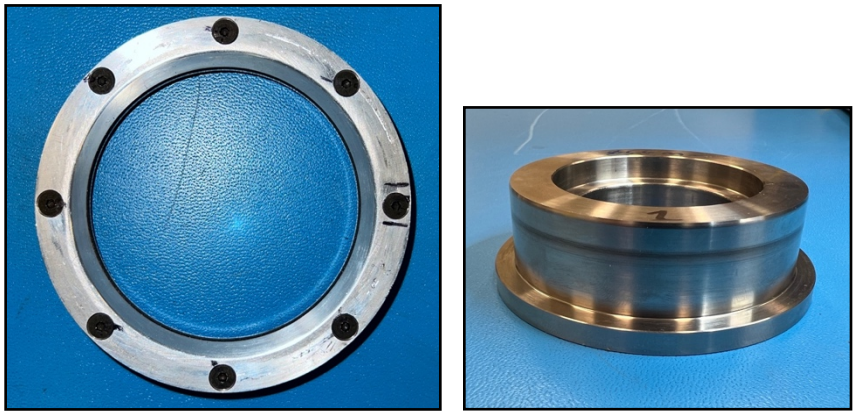

Figure 22. A CNT-metal mesh seal (ID: 66 mm) and shaft after a 160-hr compressor durability test using floating mounting. No obvious plastic deformation or wear on the seal ID and a layer of carbon transfer film on the shaft (no surface damage).

The next approach for mitigating the seal ID enlargement was to increase the number of mesh layers for a higher stiffness of the seal ID to reduce plastic deformation and a lower contact pressure on each layer of mesh to reduce wear. The first trial increased the mesh count from 20 to 40 layers, doubling the seal thickness from 1.4 mm to 2.8 mm and stiffness as well as halving the contact pressure and wear rate.

The 40-layer CNT-coated mesh seal was tested on both the bench static test rig and full-scale compressor dynamometer. The sealing efficiency on the static seal test rig and the seal ID and the mating shaft surface were examined before and after the compressor open-air and durability tests. The 40-layer CNT-coated mesh seal demonstrated much improved sealing efficiency and reliability over the 20 mesh predecessors. After the open-air compressor test, the ID diameter of the 40-layer seal increased by 70 µm, significantly less than the 370 µm increase for the 20-layer seal. The optimized assembly for the 40-layer seal also reduced variance in ID circularity. The 20-layer seals observed 70-135% increased leakage after the open-air test. In contrast, the new 40-layer seal lost less than 10% sealing efficiency after the open-air test. As a result, the 40-layer seal demonstrated 27-38% and 20-33% less leakage than the baseline labyrinth seal before and after the open-air test, respectively, as shown in Figure 23. The 40-layer seal ID was further increased by another 60 µm after the 160-hr durability test and its leakage deteriorated to be similar to that of the baseline Labyrinth seal.

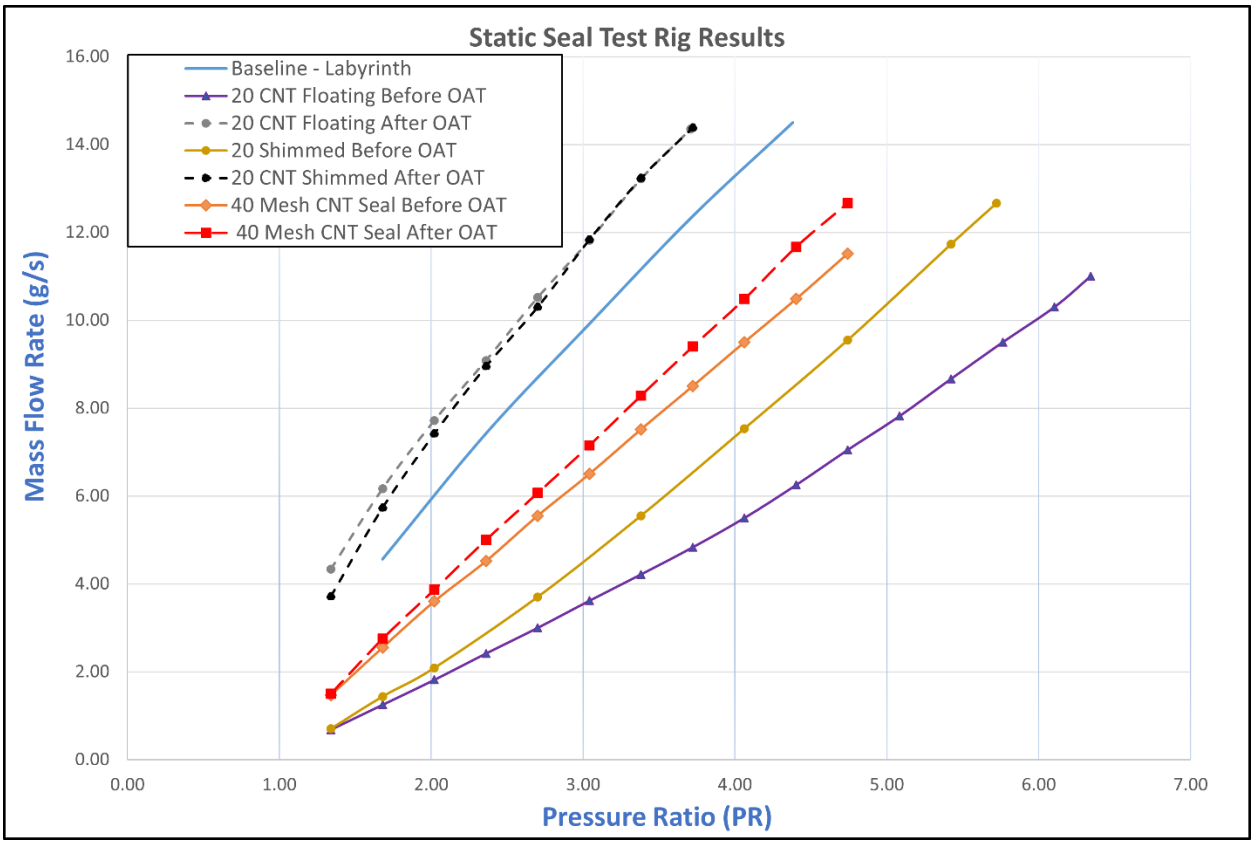

Figure 23. Static seal rig testing results of 20- and 40-layer CNT-coated mesh seals before and after the compressor open-air test. While the 20-layer seals observed 70-135% increased leakage after the open-air compressor test, the 40-layer seal lost only less than 10% sealing efficiency after. As a result, the 40-layer seal demonstrated 27-38% and 20-33% less leakage than the baseline labyrinth seal before and after the open-air compressor test, respectively.

The 40-layer CNT-coated mesh seal was then tested for durability through a 160-hr compressor durability test. The ID was slightly enlarged by 60 μm, but there was no significant surface damage on either the seal or the mating shaft, as shown in Figure 24. Again, the shaft surface was covered by a thin carbon transfer film. This is a significant improvement in durability compared with the state-of-the-art brush seals.

As shown in Figure 25, the commercial Haynes superalloy, Kevlar, and carbon fiber brush seals all had significant damage on the seal ID. In addition, the Haynes superalloy brush seal caused a lot of abrasive wear on the shaft surface. 2D scans of the worn shaft surfaces using a profiler are compared in Figure 26. The maximum wear depths are about 12 μm for the shafts after the compressor open-air and durability tests against the 20- and 40-layer CNT-coated metal mesh seals. In contrast, the wear depth was around 250 μm on the shaft tested against the Haynes superalloy brush seal.

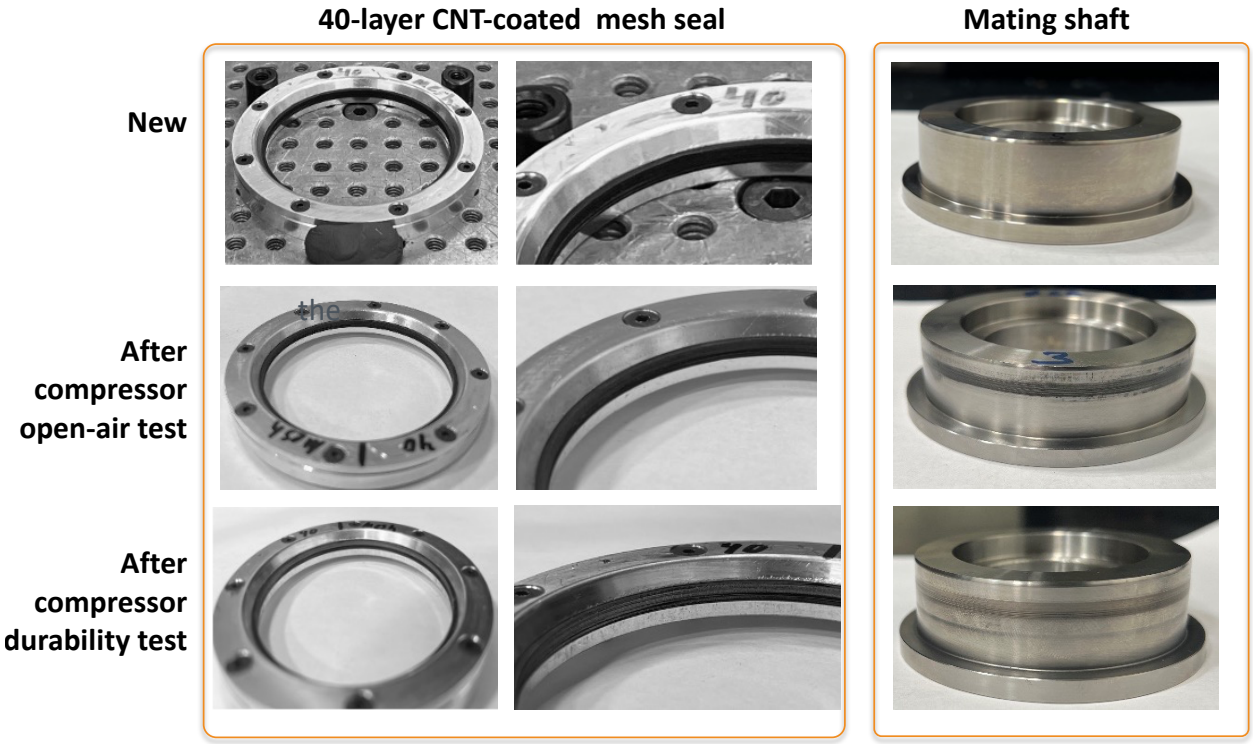

Figure 24. The 40-layer CNT-coated metal mesh seal (ID: 66 mm) and its mating shaft before and after the compressor open-air and durability tests.

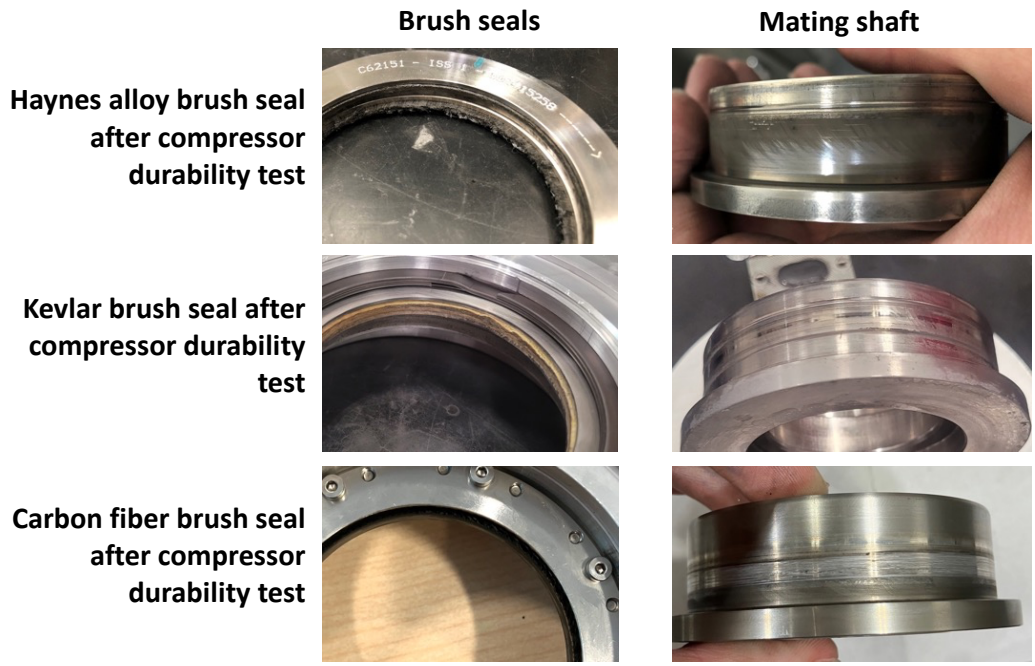

Figure 25. Significant seal ID and shaft surface damage for the state-of-the-art brush seals after compressor durability tests.

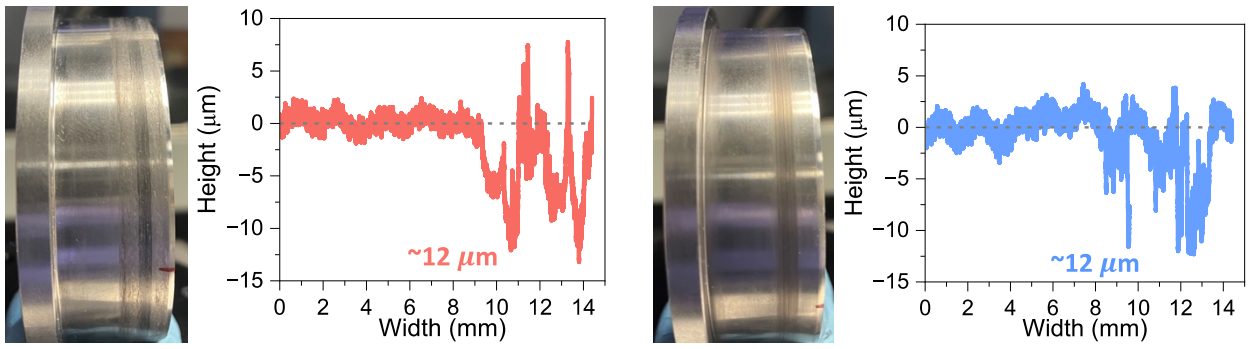

(a) Surface profiles of worn shafts tested against CNT-coated mesh seals: 20-layer (L) and 40-layer (R)

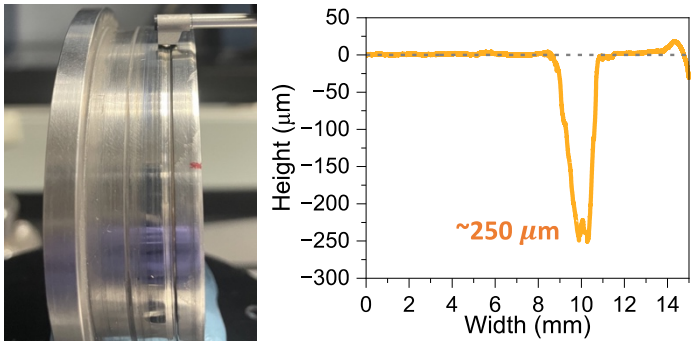

(b) Surface profiles of the worn shaft tested against the Haynes superalloy brush seal

Figure 26. Surface profiles of worn shafts after compressor durability tests.

Encouraged by the results of the 40-layer CNT-coated metal mesh seal, another trial was performed to increase the number of mesh layers to 80 for further improved yield strength and durability. Danfoss modified the seal frame to accommodate 80 layers, and ORNL produced 80+ CNT-coated mesh rings.

The 80-layer seal was then tested on both the bench static test rig and full-scale compressor dynamometer. The sealing efficiency on the static seal test rig and the seal ID and the mating shaft surface were examined before and after the compressor open-air and durability tests. Unexpectedly, the ID of the 80-layer seal was opened by 170 μm after the compressor open-air test, which was worse than the 40-layer seal. On the other hand, the ID of the 80-layer seal showed no change after a newly designed compressor durability test composed of 100 start-stop cycles of 26 minutes each (ramping to 24,000 rpm and holding for two minutes before deceleration). The sealing efficiency results were well correlated with the seal ID changes, as shown in Figure 27. The leakage flow was significantly increased after the open-air test but maintained about the same after the durability test. It is encouraging see the 80-layer CNT-coated metal mesh seal still outperformed the baseline even after the compressor durability test with 100 start-stop cycles.

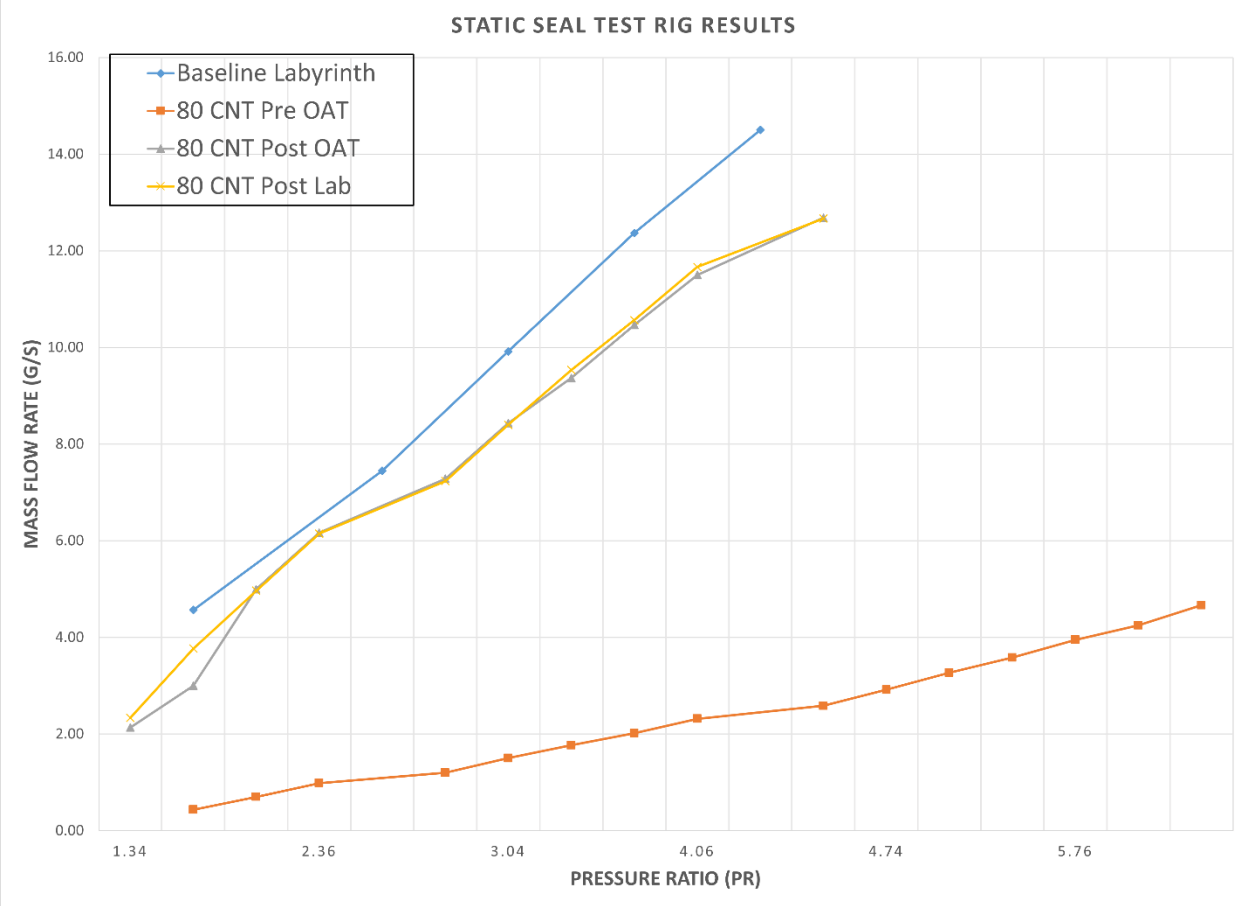

Figure 27. Static seal rig testing results of 80-layer CNT-coated mesh seal before and after the compressor open-air and durability tests.

The lack of refrigerant flow to float the CNT during the open-air test might cause a higher wear than what is otherwise seen in operation conditions. It is also suspected that the 80-layer seal was bouncing back and forth radially between the fast-spinning shaft and the volute during the open-air test leading to repeated hard-hard collisions. Higher-than-expected ID wear, likely due to such instability, was observed on another 70-layer seal in both the open-air and durability tests. Signs of abrasion on the seal's outer diameter (OD) supported the bouncing hypothesis. One solution could be designing a semi-floating mounting mechanism by introducing a cushion between the seal OD and the volute to avoid the seal bouncing and associated hard collisions with the shaft.

5. SEAL ID CONTACT MECHANICS MODELING

Finite element analysis (FEA) was conducted for the contact interface between the ID of a CNT-coated metal mesh seal and the mating shaft. A block of multi-layer CNT-coated stainless steel mesh was modeled using the representative volume element (RVE) method, as shown in Figure 28. The apparent bulk Young's modulus (E) and strength (σ_y) of the block of CNTs were assumed to be low because of the lack of strong bonding or interconnections among the CNTs.

RVE mechanical tests in FE were run to obtain the mechanical properties of the CNT-coated stainless steel mesh block in each direction. The orthotropic elasticity and plasticity were calculated as shown in Figure 29.

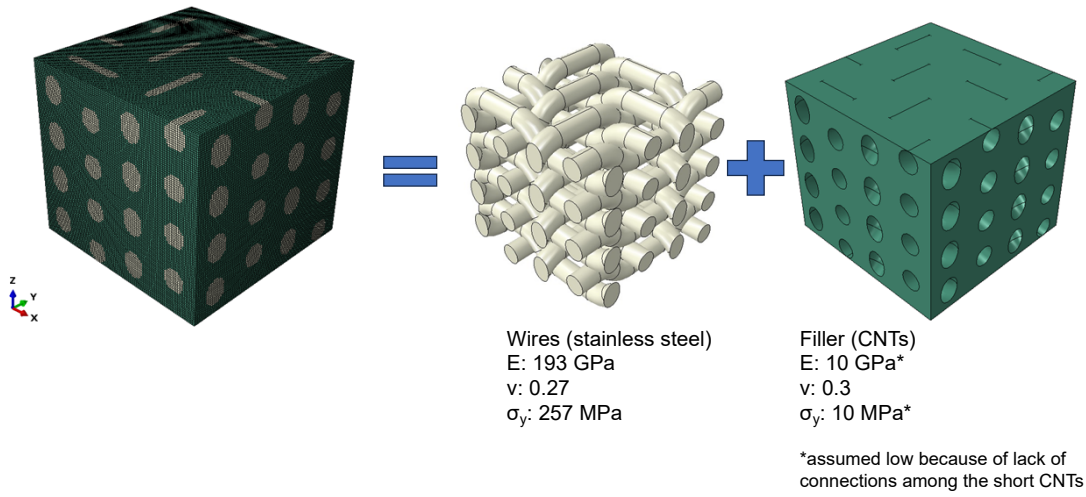

Figure 28. Stainless steel mesh modeled by representative volume element (RVE).

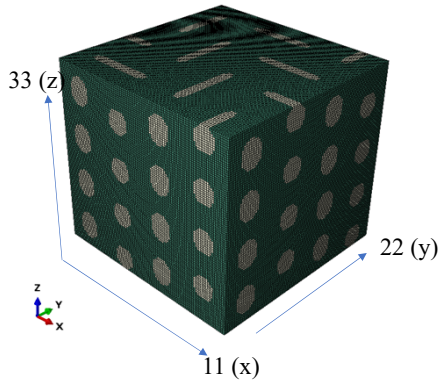

Orthotropic Elasticity of RVE

E_{11} (GPa)	E_{22} (GPa)	E_{33} (GPa)	v_{12}	v_{13}	v_{23}	G_{12} (GPa)	G_{13} (GPa)	G_{23} (GPa)
42.6	42.6	31.3	0.18	0.32	0.32	3.84	4.40	4.39

Hill's potential function for anisotropic yield (plasticity)

σ_0 (MPa)	R11	R22	R33	R12	R13	R23
47.3	1	0.996	0.937	0.268	0.350	0.349

Figure 29. Orthotropic elastic and plastic properties calculated using the RVE method for the CNT-coated stainless steel mesh block in each direction.

The full-scale model seal was constructed (see Figure 30-Left) with the mechanical properties calculated using the RVE method above. The simulation suggested that more significant deformation and larger strain would occur near the edges of the mesh ring upon compression from the shaft, as shown in Figure 30-Right. The outside layer of the mesh ring would start to yield at a relatively low compressive stress of about 50 MPa, as shown in Figure 31-Left. For such a yield stress, the calculated critical force is 144 N for 40 mesh layers assuming 1 mm wide contact. The mesh ring has a rather low shear strength of 7.3 MPa and a mere 11 N tangential force would cause yield for a 40-layer mesh ring (see Figure 31-Right). The low friction nature of the CNT-deposited transfer film on the shaft surface is critical for preventing the seal ID from yielding during the high-speed sliding. Increasing the number of mesh layers would proportionally increase the loading capacity for both compression and shear.

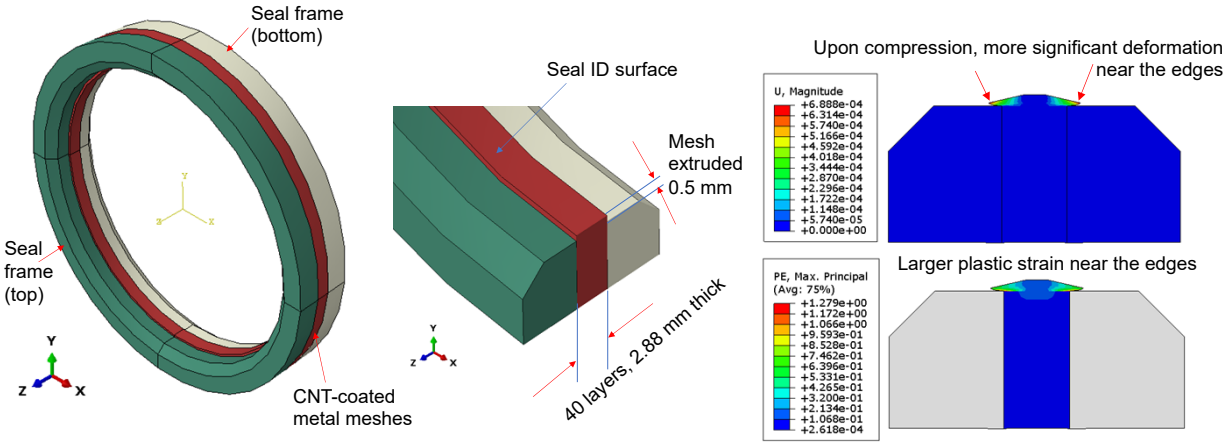

Figure 30. Full-scale model of the 40-layer CNT-coated metal mesh seal (Left, ID: 66 mm) and simulation of the meshes' plastic deformation upon compression (Right).

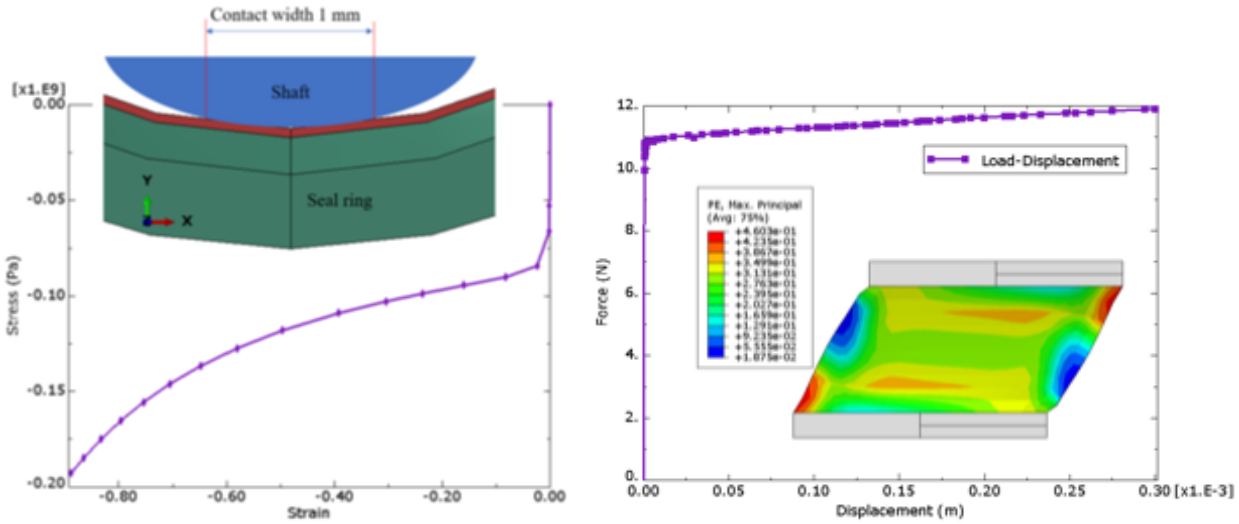

Figure 31. Calculated critical compressive stress (Left) and shear force (Right) for the 40-layer mesh seal ID. A larger number of mesh layers would increase the loading capacity for both compression and shear.

6. TECHNO-ECONOMICAL ANALYSIS

The cost of fabricating a full-scale CNT-coated metal mesh seal (66 mm ID, 40 layers of mesh) was estimated based on the prices of the materials, labor for CNT growth using CVD, and quotes for machining of the meshes and seal frame for a small batch of 100 seals, as listed in Table 7. The cost of scaled-up production would be significantly lower. The potential energy savings for using the CNT-coated metal mesh seal would be 1% for the compressor based on the 30% reduction of internal leakage flow demonstrated on the full-scale dynamometer.

Table 7. Estimated cost of fabricating a full-scale CNT-coated metal mesh seal (66 mm ID, 40 layers of mesh) based on quotes for a small batch of 100 seals.

	Stainless steel 325x325 mesh rings	CNT growth (CVD)	Seal frame (stainless steel)	Assembly	**Cost of CNT-coated metal mesh seal**
Estimated cost	$120	$120	$20	$20	**$280**

For comparison, the prices of the commercial Haynes superalloy, carbon fiber, and Kevlar brush seals are $600, $600, and $1800, respectively. The carbon fiber brush seal failed in the compressor test and the superalloy brush seal damaged the shaft, which is far more expensive than the seal for replacement. The Kevlar brush seal performed better than the other two brush seals but is three times more expensive.

7. ALTERNATE BRUSH SEAL USING COPPER MICROWIRES

In parallel to the development of the CNT-coated metal mesh seal, Danfoss issued a subcontract to Temple University to develop an alternate brush seal using Cu microwires (MWs).

The Cu MWs arrays were prepared using the following steps: 1) preparation of Si micropillar masters, 2) preparation of PMDS templates with through holes, and 3) electrodeposition of Cu MWs Using PDMS Templates. The electrodeposition was carried out in a solution of 0.6 M $CuSO_4$ and 1 M H_2SO_4 under a DC voltage of -0.4 V for two hours.

The SEM images in Figure 32 display an array of Cu MWs. The Cu MWs, with a diameter of around 20 μm, spacing of around 20 μm, and length of 250-275 μm, are well aligned and uniformly distributed on the Cu substrate. The geometry, including shape, diameter, and spacing, is replicated from the holes in the PDMS template. The length of the Cu MWs is dependent on the growth time. Due to the nonuniformity of the deposition process, the lengths of the Cu MWs showed variation and the surface of the top ends of Cu MWs is not smooth. In some cases, the Cu MWs exhibited porosity and were not perfectly solid. This could be improved by decreasing the electrolyte concentration and the voltage during growth, as well as enhancing the flowability of the electrolyte solution, such as by adding vibration to the growth setup.

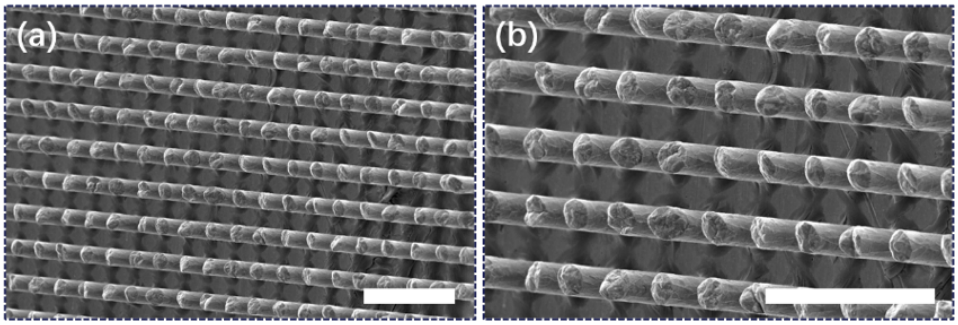

Figure 32. SEM images of the Cu MWs prepared using a PDMS template, scale bar: 100 μm.

Practical applications of 1D structures require strong bonding between them and the substrates to ensure reliability and stability. Therefore, there is great interest in quantitatively evaluating the bonding strength of the structures to their underlying substrates. Scratch tests were conducted on the Cu MWs array to evaluate its bonding strength to the substrate using a Hysitron Triboindenter (TI-900, Hysitron Inc, Minneapolis, MN, USA). The typical lateral force and normal displacement vs. time curves obtained from the scratch test are depicted in Figure 33. It can be observed that the normal displacement stabilizes at around 34 μm. Small undulations in the lateral force curve were also observed, which may be related to the spacing between Cu MWs in the array.

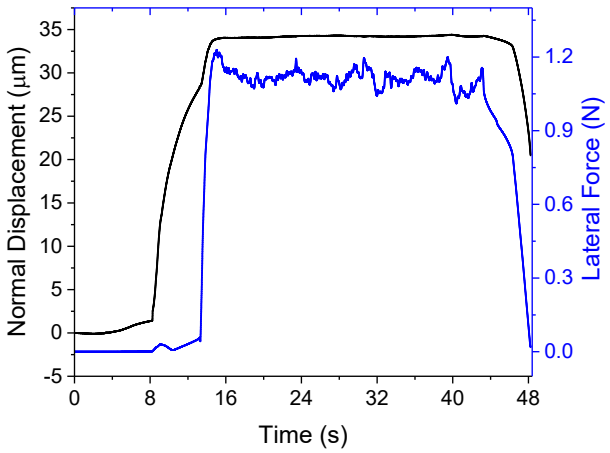

Figure 33. An example curve of the lateral force and normal displacement vs. time recorded during the scratch test.

The SEM image in Figure 34 shows the scratch scar after the scratch test. No delamination of Cu MWs from the substrate was observed, even under a normal load of 3 N. This indicates a very strong bonding between the Cu MWs array and the Cu substrate, which is extremely beneficial for practical application. In the scratch tests on a Cu MW array with a diameter of 0.4 μm and a length of up to 22 μm, it was found that the Cu MW array delaminated under a normal load of 104 mN. The adhesion energy for a 400 nm diameter Cu MW was estimated to be around 360 pJ while the adhesion energy for a 20 μm diameter Cu MW was more than 900,000 pJ. This suggests that the diameter of a 1D structure material greatly affects its bonding to the substrate.

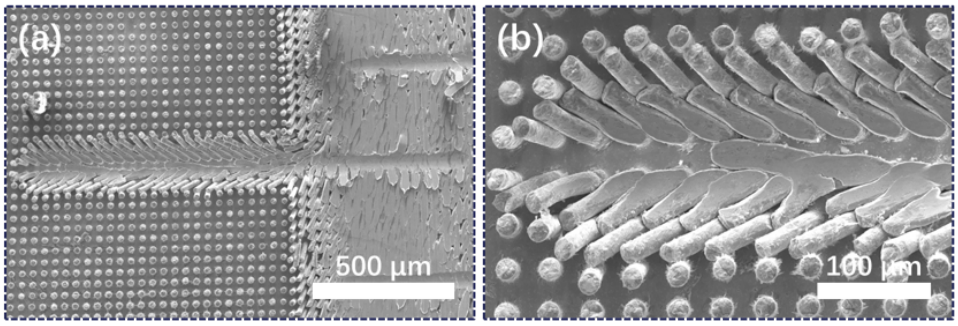

Figure 34. SEM images of the Cu MWs after the scratch test at low (a) and high (b) magnifications.

To fabricate a Cu MW brush seal, Cu MWs were first electrodeposited onto flat Cu strips that were subsequently attached to the inner wall of bronze and Al seal bases. Example seals with a 66 mm ID are shown in Figure 35.

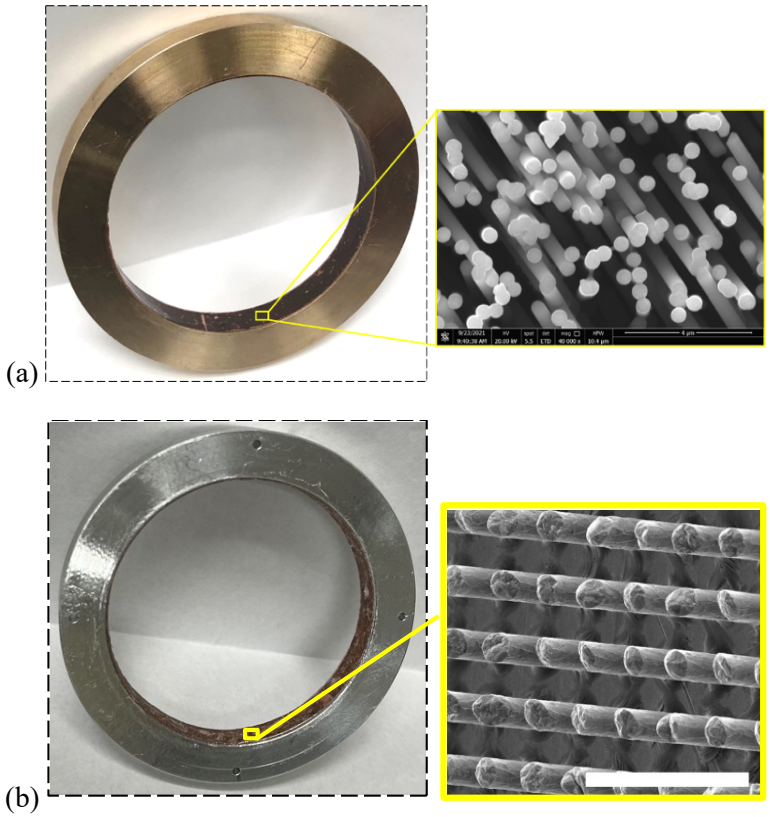

Figure 35. Examples of Cu MW brush seals (ID: 66 mm) on Cu (a) and Al (b) bases.

Danfoss tested a Cu MW brush seal on the compressor dynamometer with the seal placed in a floating configuration. High friction occurred during the initial break-in period. The compressor required a slower ramp speed to allow torque to build over a greater amount of time. Afterward, the compressor passed the open-air test and the seal ID was enlarged by 50 µm. The compressor durability test included a 48-hour Speedline test at 27,000 rpm for pressure ratios between 2.3 and 2.9. Five steady-state data points were collected, revealing comparable performance to the industry standard labyrinth seal.

An additional static seal test confirmed these results. It was found that a portion of the copper strip delaminated from its structural ring from the 48-hour compressor test. Another static seal test was then conducted after re-adhering the strip back. The repaired Cu MW seal showed better sealing than the labyrinth baseline. Results demonstrated 30% and 10% less leakage for the Cu MW brush seal compared with the baseline after open-air and compressor durability tests, respectively, as shown in Figure 36.

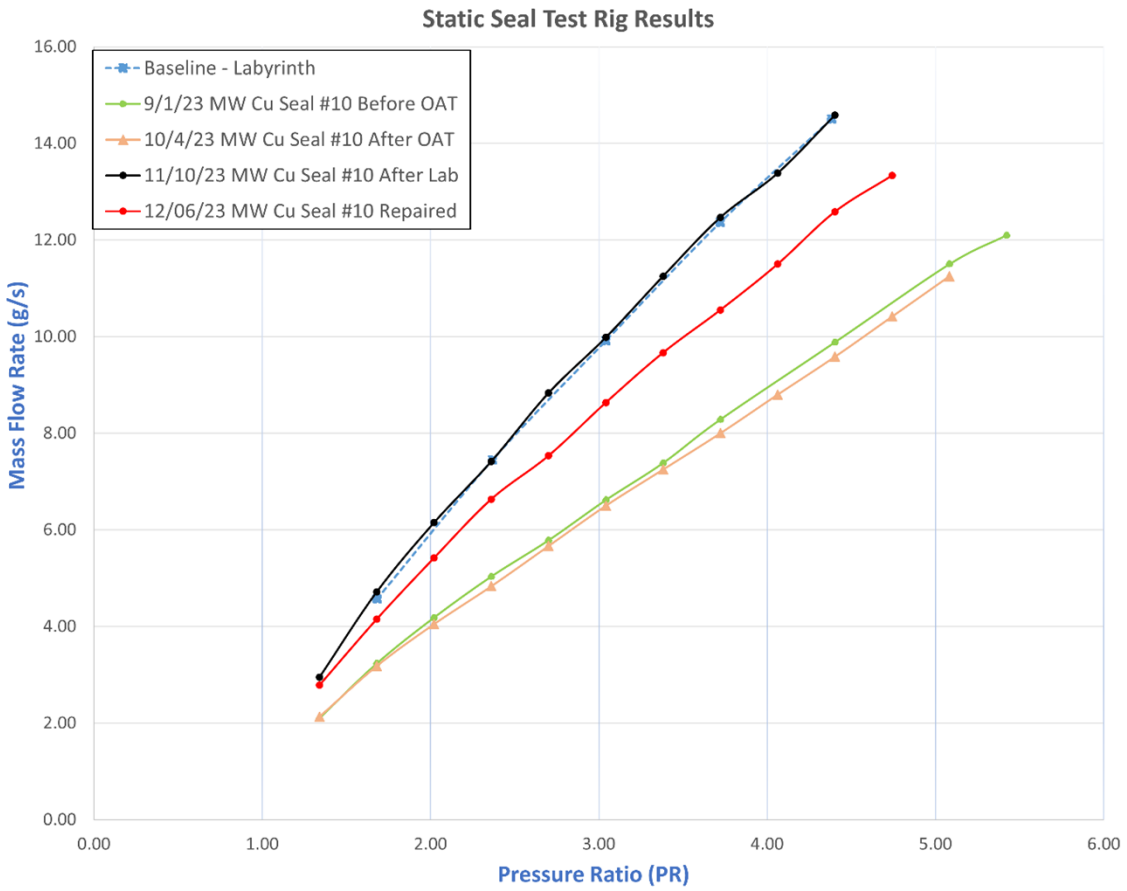

Figure 36. Static seal rig testing results of a Cu MW brush seal demonstrated 30% and 10% less leakage than the baseline labyrinth seal after the compressor open-air and durability tests, respectively.

8. CONCLUSIONS

A novel concept of CNT-coated metal mesh hybrid seals was invented in this collaboration between ORNL and Danfoss. A CVD-based CNT growth process was first developed for stainless steel meshes and then scaled up for coating large-size (100x100 mm) mesh sheets. The morphology, crystallinity, and resistance to sCO_2 corrosion of the CNTs were characterized. Full-scale experimental seals were designed, fabricated, and tested on both static seal rig and compressor dynamometer. The seal design and mounting method were modified multiple times based on the testing results, post-test characterization, and contact mechanics simulation for improved sealing efficiency and durability. Superior gas sealing efficiency and better shaft surface protection were demonstrated for both the CNT-coated metal mesh seal compared the baseline labyrinth seal and state-of-the-art brush seals. The CNT-metal mesh seal is low-cost and scalable and can potentially benefit wide applications, including CSP and other power generation, marine, automotive, and HVAC. In parallel, an alternate brush seal using Cu MWs was developed at Temple under a subcontract and also showed encouraging results in the seal tests.

ACKNOWLEDGMENTS

Research was sponsored by the Solar Energy Technologies Office, Office of Energy Efficiency and Renewable Energy, United States Department of Energy (DOE). The authors thank K. Cooley and D. Fleming from ORNL for assisting in the CVD setup and machining of metal meshes and seal bases and S. Jang from ORNL for surface profiling of the worn shafts.

REFERENCES

1. J.G., Ferguson, "Brushes as High Performance Gas Turbine Seals," ASME Paper No. 88-GT-182.
2. R.E. Chupp, et al., "Sealing in Turbomachinery," NASA Report No. NASA/TM 2006-214341.
3. S. Dinc, et al., "Fundamental Design Issues of Brush Seals for Industrial Applications," ASME J. Turbomach., 124 (2002), 293–300.
4. T. Held, *Rotating Seals for Supercritical CO2 Power Cycle Turbomachinery, Consulting report*. 2020.
5. H. Zimmermann, K.H. Wolff, *Comparison Between Empirical and Numerical Labyrinth Flow Correlations*. in *ASME 1987 International Gas Turbine Conference and Exhibition*. 1987.
6. Egli, A., *he Leakage of Steam through Labyrinth Seals.* Transactions of the ASME, 1935(57).
7. D.W.V. Childs, M. John, *Annular Gas Seals And Rotordynamics Of Compressors And Turbines*. in *Proceedings of 26th Turbomachinery Symposium*. 1997. Texas A&M University, College Station, TX.
8. R.E. Chupp, et al., *Sealing in Turbomachinery.* Journal of Propulsion and Power, 2006. 22(2): p. 313-349.
9. Arash, B.; Wang, Q.; Varadan, V. K. Mechanical properties of carbon nanotube/polymer composites. Scientific Reports 2014, 4 (1), 6479, DOI: 10.1038/srep06479.
10. Wang, Q.; Yuan, H.; Zhang, M.; Yang, N.; Cong, S.; Zhao, H.; Wang, X.; Xiong, S.; Li, K.; Zhou, A. A Highly Conductive and Supercapacitive MXene/N-CNT Electrode Material Derived from a MXene-Co-Melamine Precursor. ACS Applied Electronic Materials 2023, 5 (5), 2506-2517, DOI: 10.1021/acsaelm.2c01768.
11. Pour, G. B.; Ashourifar, H.; Aval, L. F.; Solaymani, S. CNTs-Supercapacitors: A Review of Electrode Nanocomposites Based on CNTs, Graphene, Metals, and Polymers. Symmetry 2023, 15 (6), 1179.
12. Wieland, L.; Li, H.; Rust, C.; Chen, J.; Flavel, B. S. Carbon Nanotubes for Photovoltaics: From Lab to Industry. Advanced Energy Materials 2021, 11 (3), 2002880, DOI: https://doi.org/10.1002/aenm.202002880.
13. Aalam, S. M.; Sarvar, M.; Sadiq, M.; Ali, J. A Highly Sensitive Surface-Modified Porous Carbon Nanotube-Based Sensor for Ammonia Gas Detection. ACS Omega 2024, 9 (4), 4486-4496, DOI: 10.1021/acsomega.3c07244.

14. Elias, L.; Shibli, S. M. A. Surface-Modified Carbon Nanotubes for Hydrogen Storage. In Surface Modified Carbon Nanotubes Volume 2: Industrial Applications; American Chemical Society: 2022; Chapter 7, pp 151-173.

15. Anikina, E.; Banerjee, A.; Beskachko, V.; Ahuja, R. Li-Functionalized Carbon Nanotubes for Hydrogen Storage: Importance of Size Effects. ACS Applied Nano Materials 2019, 2 (5), 3021-3030, DOI: 10.1021/acsanm.9b00406.

16. Li, Q.; Zhu, Z.; Wang, Y.; Wang, H.; Li, J.; Ma, X. Unprecedented gas separation performance of ITTB/CNT nanocomposite membranes at low temperature by strong interfacial interaction enhanced rigidity. Journal of Membrane Science 2021, 636, 119590, DOI: https://doi.org/10.1016/j.memsci.2021.119590.

17. Kumara, C.; Lance, M. J.; Qu, J. Macroscale superlubricity by a sacrificial carbon nanotube coating. Materials Today Nano 2023, 21, 100297, DOI: https://doi.org/10.1016/j.mtnano.2022.100297.

18. Baykara, M. Z.; Vazirisereshk, M. R.; Martini, A. Emerging superlubricity: A review of the state of the art and perspectives on future research. Applied Physics Reviews 2018, 5 (4), 041102, DOI: 10.1063/1.5051445.

19. Zhang, R.; Ning, Z.; Zhang, Y.; Zheng, Q.; Chen, Q.; Xie, H.; Zhang, Q.; Qian, W.; Wei, F. Superlubricity in centimetres-long double-walled carbon nanotubes under ambient conditions. Nature Nanotechnology 2013, 8 (12), 912-916, DOI: 10.1038/nnano.2013.217.

20. Pirard, S. L.; Douven, S.; Pirard, J.-P. Large-scale industrial manufacturing of carbon nanotubes in a continuous inclined mobile-bed rotating reactor via the catalytic chemical vapor deposition process. Frontiers of Chemical Science and Engineering 2017, 11 (2), 280-289, DOI: 10.1007/s11705-017-1635-1.

21. Li, Y.; Xu, G.; Zhang, H.; Li, T.; Yao, Y.; Li, Q.; Dai, Z. Alcohol-assisted rapid growth of vertically aligned carbon nanotube arrays. Carbon 2015, 91, 45-55, DOI: https://doi.org/10.1016/j.carbon.2015.04.035.

22. Kim, B.; Chung, H.; Chu, K. S.; Yoon, H. G.; Lee, C. J.; Kim, W. Synthesis of vertically-aligned carbon nanotubes on stainless steel by water-assisted chemical vapor deposition and characterization of their electrochemical properties. Synthetic Metals 2010, 160 (7), 584-587, DOI: https://doi.org/10.1016/j.synthmet.2009.12.008.

23. Sano, N.; Yamamoto, S.; Tamon, H. Cr as a key factor for direct synthesis of multi-walled carbon nanotubes on industrial alloys. Chemical Engineering Journal 2014, 242, 278-284, DOI: https://doi.org/10.1016/j.cej.2013.12.073.

24. Zhuo, C.; Wang, X.; Nowak, W.; Levendis, Y. A. Oxidative heat treatment of 316L stainless steel for effective catalytic growth of carbon nanotubes. Applied Surface Science 2014, 313, 227-236, DOI: https://doi.org/10.1016/j.apsusc.2014.05.189.

25. Hashempour, M.; Vicenzo, A.; Zhao, F.; Bestetti, M. Direct growth of MWCNTs on 316 stainless steel by chemical vapor deposition: Effect of surface nano-features on CNT growth and structure. Carbon 2013, 63, 330-347, DOI: https://doi.org/10.1016/j.carbon.2013.06.087.

26. J. Qu, C. Kumara, P.A. Menchhofer, “A superlubricity coating composed of vertically-aligned carbon nanotubes,” U.S. Patent Application 62/931,246, 2019.

27. J. Qu, C. Kumara, T. Li, “A high-efficiency seal composed of carbon nanotubes,” U.S. Patent Application, 18/371,817, 2023.